## APPLIED PHYSICS REVIEWS—FOCUSED REVIEW

# Physics and materials challenges for lead-free solders

K. N. Tu
*Department of Materials Science and Engineering, University of California, Los Angeles, California 90095-1595*

A. M. Gusak
*Department of Theoretical Physics, Cherkasy State University, Cherkasy, Ukraine*

M. Li
*Institute of Materials Research and Engineering, Singapore 119260, Singapore*

(Received 17 May 2002; accepted 29 August 2002)

At present, the electronic industry is actively searching for Pb-free solders due to environmental concerns over Pb-containing solders. Solder joints are widely used to bond chips to their substrates for electrical connection and packaging. Lacking reliability data, many electronic companies will be reluctant to adopt Pb-free solders in the advanced products. Hence, it is timely to review our understanding of structure-property relationship and potential reliability issues of Pb-free solders. A brief history of solder joint processes in electronic manufacturing is presented to serve as a background for the review. It emphasizes the unique phenomenon of spalling of interfacial intermetallic compound in solder reactions. Challenges for Pb-free solders from the point of view of physics and materials are given since the reliability issues of solder joints will remain with us when advanced Cu/low *k* dielectric interconnect technology is introduced into microelectronic devices. © *2003 American Institute of Physics.* [DOI: 10.1063/1.1517165]

### TABLE OF CONTENTS



## I. INTRODUCTION

Microelectronic packaging is about how to connect the circuitry on a Si chip to the outside world. Both wire bonding and solder bumping technologies have been used. The trend in microelectronic packaging is toward wider use of solder bumping. The advantage of solder bumping is that a large number of tiny solder bumps can be made into an area array on a chip surface as input/output (I/O) interconnections. Today, the diameter of solder bumps is 100 $\mu$m and the pitch between them is 100 $\mu$m, so on a 1 cm$^2$ chip surface, we can have 2500 I/O bumps. If the bump diameter and pitch are reduced to 50 $\mu$m, we can have 10 000 bump/cm$^2$. This aerial density meets the projected I/O requirement for the next 10 years given by the Semiconductor Industry

 

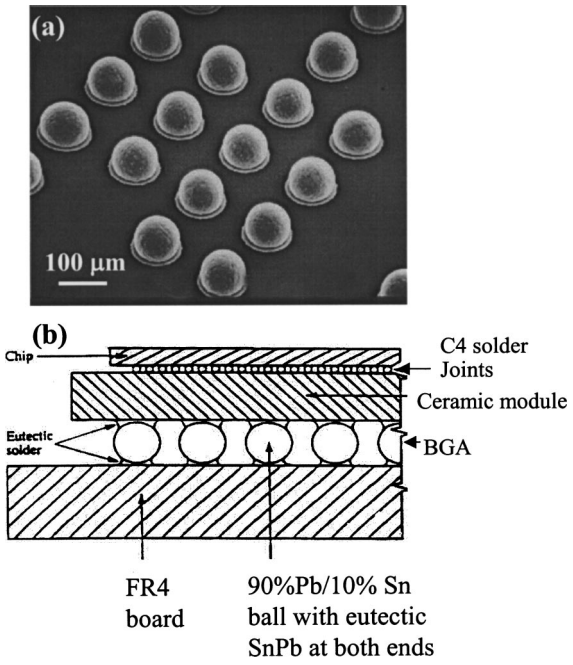


FIG. 1. (a) Area array of solder balls on a Si chip surface (courtesy of W. J. Choi, UCLA). (b) Cross section of two-level packaging: chip-to-ceramic module and ceramic module-to-polymer board, where C-4 solder joints are controlled-collapse-chip-connection solder joints and BGA is ball-grid-array (after Ref. 3).

Association.[1] Figure 1(a) shows a scanning electron microscopic image of an array of solder bumps on a Si surface.

Solder alloy of 95 wt % Pb and 5 wt % Sn (95Pb5Sn) has been used as solder bumps on Si chip surfaces in mainframe computers.[2] To join a chip to a ceramic module as shown in Fig. 1(b), the chip is flipped upside down, i.e., the side having the active very-large-scale integration (VLSI) of the device is downward. It is known as flip chip technology. Then the ceramic module is joined to a printed circuit board using a second set of solder bumps, which are eutectic SnPb solder (or a composite solder) and the bump size is much bigger; see Fig. 1(b). Eutectic SnPb solder (38 wt % Pb and 62 wt % Sn) is used in the second set because it has a much lower melting point (183 °C) than 95Pb5Sn solder (320 °C). Hence the high-Pb solder bumps will not melt during the joining of eutectic bumps. This is a two-level packaging scheme used in mainframe computers, first chip to ceramic and then ceramic to polymer.[2,3]

When low-cost large-volume consumer electronic products are up graded by using advanced chips for better performance, more I/O will be needed so that flip chip technology will become attractive. But the high-cost ceramic module should be removed so chips can be joined directly to polymer boards or cards. To do so, the high melting point of 95Pb5Sn solder can no longer be used because of the low glass transition temperature of polymers. While the eutectic SnPb meets the low melting point requirement, the electronic industry is, however, searching for Pb-free solders to replace Pb-containing solders because of environmental benign manufacturing.[4,5]

Besides environmental concerns, Pb-containing solders may have minute amounts of $Pb^{210}$ isotope. It decays to Bi. During the decay, it emits alpha particles. When these particles pass through a Si device, they generate electrons and holes. Before these charge carriers recombine, they may affect the charge stored in the capacitors (memory units) of the device, leading to ''soft error'' failure.[6] To prevent this problem, Pb-free solder is one of the solutions.

In the United States, there are four anti-Pb bills pending in Congress. Europe has the Waste Electrical and Electronic Equipment (WEEE) directive to ban the use of Pb in consumer electronics by 2006.[4] In Japan, all major consumer electronic manufacturers have announced accelerated schedules for Pb-free products.[4]

One of the U.S. anti-Pb bills is from the Environmental Protection Agency.[4,5] The National Electronics Manufacturing Initiative (NEMI) has a Pb-free assembly project to address solutions of Pb-free electronics manufacturing. NEMI has recommended replacing eutectic SnPb alloys by eutectic SnAgCu alloys in reflow processing and eutectic SnCu alloys in wave soldering.[5] The term ''reflow'' means that a solder joint experiences a temperature between room temperature and a high temperature which is about 30 °C above the melting point of the solder, with a duration of about 1 min above the melting point. In electronic manufacturing, at least two reflows are required. The first reflow forms an area array of solder bumps on a chip surface, and the second reflow bonds the chip to a substrate. Actually, in manufacturing the number of reflows could be more than two, e.g., due to testing and repair of chips. The term ''wave soldering'' means passing a packaging board over a fountain of molten solder to achieve joining using pin-through-hole technology. Due to capillary force, the molten solder will run into the plated through hole (holes plated with Cu and immersion in Sn) in the board and join a pin which has been inserted into the hole. This technology is required for the packaging of devices used in military equipment for high reliability.

To replace the SnPb solders, we must consider what the key processes in solder joining are. To yield a solder joint, the solder must wet a conductor, typically Cu, and the most challenging issue is how to control the wetting reaction. This is because the conductors on a Si chip are thin metal films. During wetting reactions, the molten solder can consume a 1 $\mu$m thick Cu thin film in less than 1 min. However, in manufacturing a device or computer, the solder joints are required to go through several ''reflows'' or several wetting reactions. When the thin film is consumed, the interface of the solder joint becomes very weakened mechanically due to the phenomenon of ''spalling'' (to be discussed below). Hence, the solder–thin film reaction is the most critical issue in electronic manufacturing.

Since SnPb solders have been used for a long time, we must examine the unique properties of Pb in SnPb solders. First, Pb provides ductility and a shiny surface. Second, it lowers the surface and interfacial energies of the solder. The eutectic SnPb solder has a very low wetting angle of 11° on Cu, and the wetting angle of pure Sn on Cu is 35°.[7] Third, the eutectic SnPb solder has a low melting temperature of 183 °C compared to the melting points of 232 and 327 °C of pure Sn and Pb, respectively. Fourth, the high-Pb solder of 95Pb5Sn has a very narrow temperature gap of about 10 °C,

TABLE I. Binary eutectic solders.

| System | Eutectic temperature (°C) | Eutectic composition (wt % of the 2nd element) |
|---|---|---|
| Sn–Cu | 227 | 0.7 |
| Sn–Ag | 221 | 3.5 |
| Sn–Au | 217 | 10 |
| Sn–Zn | 198.5 | 9 |
| Sn–Pb | 183 | 38.1 |
| Sn–Bi | 139 | 57 |
| Sn–In | 120 | 51 |

between its liquidus and solidus points, so it can be used as a high temperature solder. Therefore, a high–low combination of the high-Pb and the eutectic SnPb solders can be applied in two-level packaging as shown in Fig. 1(b).

At present, most Pb-free solders are Sn based. A special class of Pb-free solders is the binary eutectic alloys of Sn and noble metals (Cu, Ag, and Au) shown in Table I.[8] The ternary eutectic SnAgCu alloy has received much attention.[9–13] For solder, a eutectic alloy is preferred since it has a single melting point and the entire joint will melt or solidify at the eutectic temperature. Other elements such as Bi, In, Zn, Sb, and Ge have been considered as eutectic partners with Sn, but they are not as common as noble metals. The eutectic composition and temperature of several Pb-free solder alloys are compared with those of eutectic SnPb in Table I. The Sn–Au alloy at 80 wt % of Au has a eutectic point of 280 °C. At the moment it is the only alloy that could be considered a high temperature Pb-free solder, yet it is known to have poor reflow behavior besides its cost.

### A. Solder reactions

Figure 2 is a cross-sectional scanning electron microscopy (SEM) image of the interface between eutectic SnPb and thick Cu foil.[14,15] The interfacial reaction forms intermetallic compounds (IMCs) of $Cu_6Sn_5$ in a scallop-type morphology. When the sample was deep etched to remove the Pb (the Sn also goes away), a much clearer three-dimensional (3D) image of the scallop-type IMC was revealed. Figure 3 is a series of images of the scallops formed over different periods at 200 °C, taken at the same magnification.[14] The important finding here is that the growth of scallops is accompanied by ripening. They grow bigger but there are fewer in the same area. It is nonconservative ripening, since the total volume of the scallops has increased over time. The scallop-type IMC morphology is common in solder reactions. Besides the reaction between eutectic SnPb and Cu, it has been observed in wetting reactions between eutectic SnPb and Ni,[16] between eutectic SnAg and Cu,[15] and also between eutectic SnBi and Cu.[15] We note that the scallop-type morphology of growth is very different from the layer-type morphology of IMC growth observed in solid state reactions, e.g., silicide formation between thin metal films and Si.

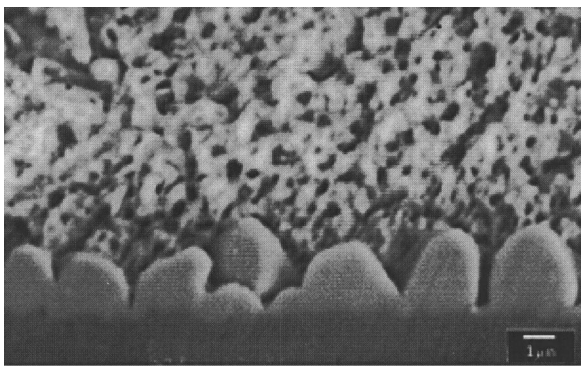

FIG. 2. Cross-sectional SEM image of scallop-type IMC formation at the interface between eutectic SnPb and a thick Cu foil (after Refs. 3 and 7).

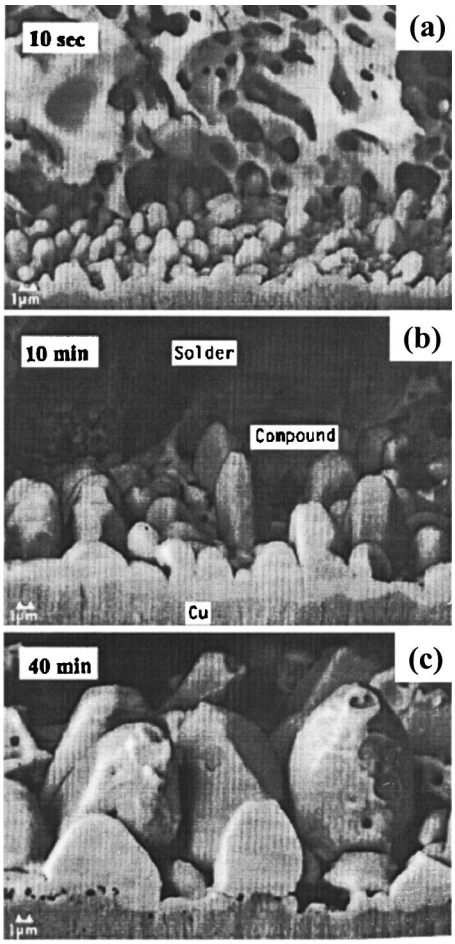


FIG. 3. Cross-sectional SEM 3D images of the growth of scallop-type IMC between eutectic SnPb and a Cu foil at 200 °C for (a) 1, (b) 10, and (c) 40 min (after Refs. 14 and 15).

If the thick Cu foil is replaced by a thin Cu film, a dramatic change in the IMC morphology occurs. Figure 4 shows a cross-sectional SEM image of eutectic SnPb solder on a bilayer of thin film of 870 nm Cu/100 nm Ti on an oxidized Si wafer.[17,18] After 10 min at 200 °C, the scallop-type $Cu_6Sn_5$ IMC no longer exists, but rather the IMCs have become spheroidal and some of them have left the substrate and spalled into the solder. This is unexpected because when the Cu film is completely consumed by the solder, we expect the interfacial reaction to stop since there is no more Cu. Yet the ripening reaction continues among the scallops. It changes to conservative ripening under constant volume, driven by decreasing surface, and it transforms the hemi-

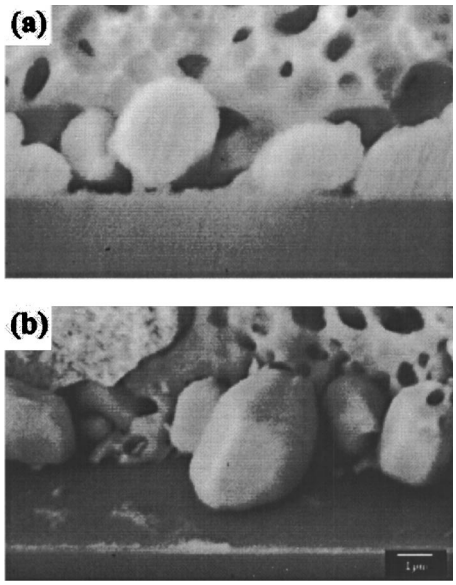


FIG. 4. Cross-sectional SEM image of the formation of spheroid-type $Cu_6Sn_5$ at the interface between eutectic SnPb and 870 nm Cu/100 nm Ti thin film underbump metallization after 10 min at 200 °C. (a) Two dimensional (2D) image and (b) 3D image after etching away the solder (after Refs. 3, 17, and 18).

spherical scallops into spheroids. The spheroids have a 180° wetting angle on the Ti surface. Since there is no adhesion between them, the spheroids can detach easily from the Ti surface and migrate into the molten solder. This is the phenomenon of ''spalling'' of thin film IMC.[19] When it occurs, the molten solder has very little interaction with the unwetted substrate and dewetting of the joint can occur. Figure 5 is a set of schematic diagrams of the sequence of ripening, spalling, and dewetting in a solder–thin film reaction.[7] In the following, we shall discuss why the spalling has become a recurring phenomenon in flip chip technology.

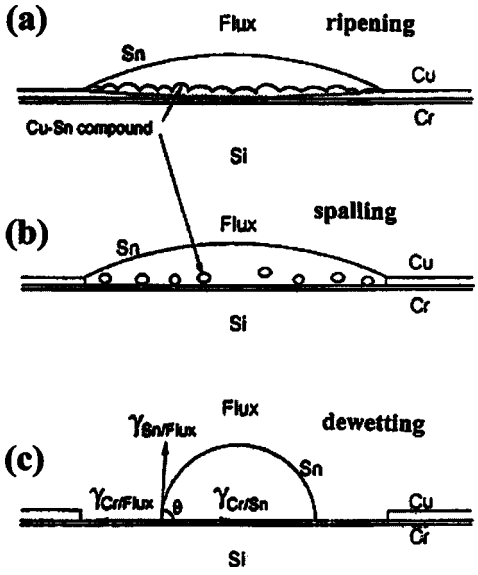


FIG. 5. Schematic diagrams depicting the phenomena of (a) ripening among scallop-type IMCs, (b) spalling of spheroid-type IMCs, and (c) dewetting of the solder cap on a thin film underbump metallization (after Ref. 3).

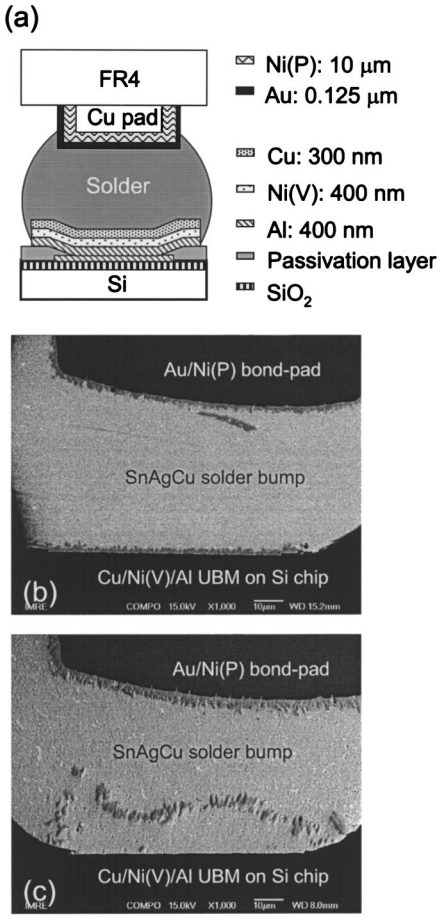


FIG. 6. (a)Schematic diagram depicting metallurgical structures across a real solder joint. The UBM on the chip side consists of 300 nm of Cu/400 nm of Ni(V)/400 nm of Al. The thick metallic bond pad on the board side, across the solder bump, consists of 125 nm of Au/10 $\mu$m of Ni(P)/a very thick Cu pad. (b) Cross-sectional SEM image of such a solder joint which bonded a chip (the bottom) to a board (the top). The formation of a scallop-type IMC at the two solder interfaces can be seen. (c) SEM image of the joint after 10 reflows. The IMC on the chip side has spalled into the solder (after Ref. 8).

## II. INTERFACIAL REACTIONS AND SPALLING OF A THIN FILM IMC

Figure 6(a) is a schematic diagram depicting the metallurgical structures across a real solder joint. The thin film under-bump metallization (UBM) on the chip side consists of 300 nm of Cu/400 nm of Ni(V)/400 nm of Al. The thick metallic bond pad on the board side, across the solder bump, consists of 125 nm of Au/10 $\mu$m of Ni(P)/a very thick Cu pad. The Cu film and the Au film are, respectively, the surface metallization on the chip side and the board side, and between them is the eutectic SnAgCu solder bump. Figure 6(b) shows a cross-sectional scanning electron microscopy image of such a solder joint which bonded a chip (the bottom) to a board (the top). The formation of scallop-type IMC at the two solder interfaces can be seen. Figure 6(c) shows the same image of the joint after 10 reflows. The IMC on the chip side has spalled into the solder.

In the following, we shall review a series of reactions between molten solder and thin metal films in electronic packaging technology, and we shall see that the spalling is a

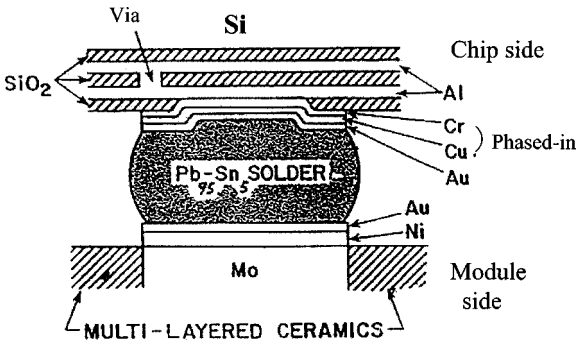


FIG. 7. Schematic diagram of a 95Pb5Sn solder bump joining the thin film Au/Cu/Cu–Cr on a Si chip to a ceramic module.

recurring phenomenon and it remains a very challenging issue for Pb-free solder.

### A. No spalling in high-Pb solder on Au/Cu/Cu–Cr thin films

First, we review the controlled-collapse-chip-connection (C-4) solder joint used in a mainframe computer.[2] Figure 7 is a schematic diagram of a 95Pb5Sn solder ball that joins a thin film metallization which consists of 100 nm of Au/500 nm of Cu/300 nm of codeposited Cu–Cr to a ceramic module. We note that each of trilayer of Au/Cu/Cu–Cr has been chosen for a particular reason. Since solder does not wet the very-large-scale-integrated Al wires on Si, Cu is selected for its reaction with Sn to achieve solder bonding. But because Cu does not adhere well to the interlayer dielectric $SiO_2$ and the oxidized Al surface, Cr is selected as a glue layer for the adhesion to $SiO_2$ and Al. Yet Cu and Cr have poor adhesion to each other, so the phased-in Cu–Cr or codeposited Cu–Cr was developed to improve the adhesion. Because Cr and Cu are immiscible, their grains form an interlocking microstructure when they are codeposited. Finally, Au is used as a surface coating to prevent the oxidation or corrosion of Cu and to enhance solder wetting.

Figure 8 shows bright-field cross-section transmission electron microscopy (TEM) images of the trilayer thin film structure. A selected area diffraction pattern of the Cu–Cr layer can be indexed as a mixture of reflection rings of Cu and Cr. A high resolution TEM image of the mixed Cu and Cr layer is shown in Fig. 9, in which the lattice of Cu or Cr can be identified. When a molten high-Pb solder of 95Pb5Sn wets this trilayer thin film metallization, it dissolves the Au, forms $AuSn_4$ compound particles in the solder, and forms a $Cu_3Sn$ compound on the Cu–Cr layer. The metallurgical structure is stable up to several reflows so the C-4 flip chip solder joints have been used for over 30 years in mainframe computers.

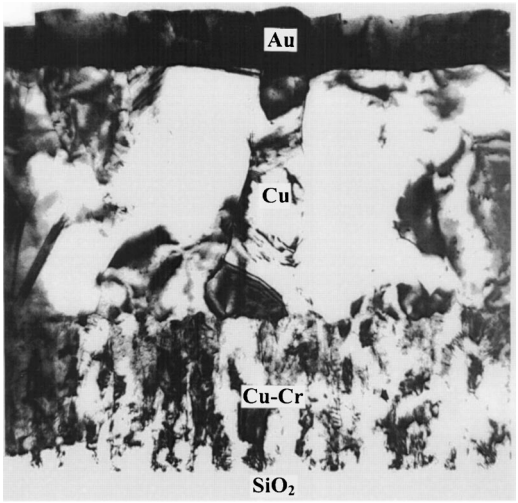


FIG. 8. Bright-field cross-sectional TEM images of a trilayer thin film structure of Au/Cu/Cu–Cr (courtesy of N. Wang, Department of Physics, Hong Kong University of Science and Technology, Hong Kong) (after Ref. 3).

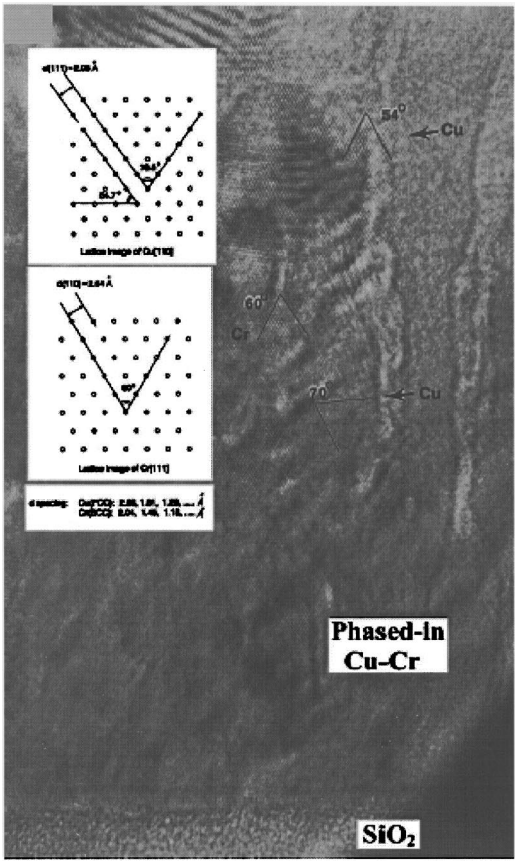


FIG. 9. High resolution TEM image of the mixed Cu and Cr layer in which the lattices of Cu and Cr are identified (courtesy of N. Wang, Department of Physics, Hong Kong University of Science and Technology, Hong Kong) (after Ref. 3).

### B. Spalling in eutectic SnPb solders on Au/Cu/Cu–Cr thin films

Due to the need for advanced chips in consumer electronic products and the need for more I/O interconnections on a chip surface, flip chip technology has lately gained attention in electronic manufacturing. In these products, chips are joined to polymer boards and cards. The low melting eutectic SnPb which can be reflowed at 220 °C is suitable. When the eutectic SnPb solder reacts with Cu at 220 °C, the reaction product is $Cu_6Sn_5$ rather than $Cu_3Sn$. This is in agreement with the ternary phase diagrams of Sn–Pb–Cu shown in Fig. 10. The $Cu_6Sn_5$, however, is morphologically unstable on the Cu–Cr surface, leading to spalling. Figure 11

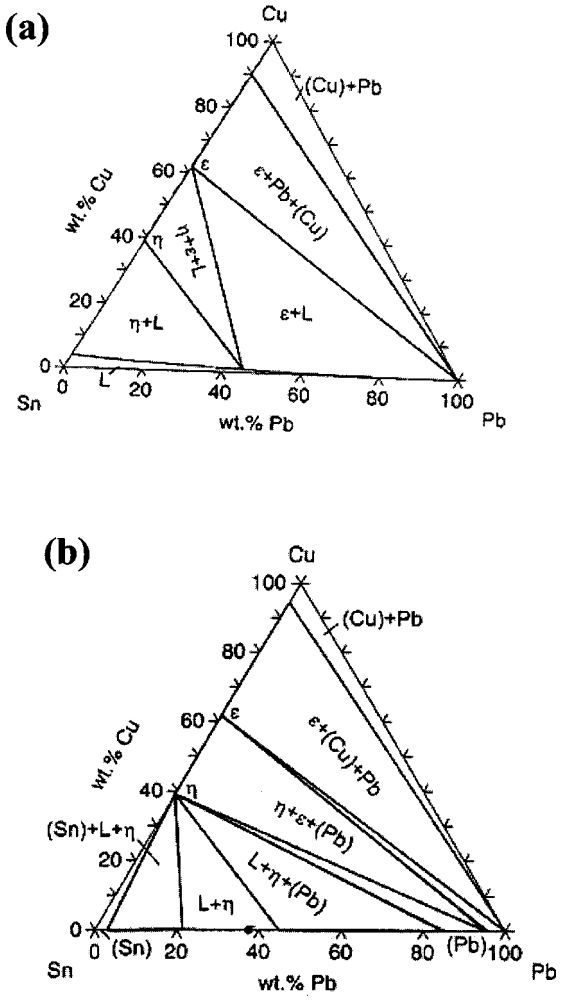


FIG. 10. Ternary phase diagram of Sn–Pb–Cu at (a) 170 and (b) 200 °C; the diagram at 220 °C is basically the same.

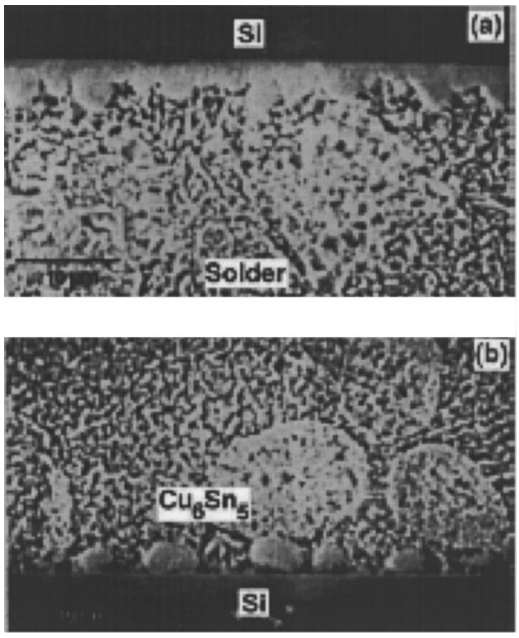


FIG. 11. Cross-sectional SEM image of a eutectic SnPb solder bump sandwiched between two Si chips with Au/Cu/Cu–Cr films. After 20 min at 200 °C, the $Cu_6Sn_5$ spheroids have departed from the bottom surface and moved towards the upper interface, assisted by gravitational force (after Ref. 18).

shows a cross-sectional SEM image of a eutectic SnPb solder bump sandwiched between two Si chips with Au/Cu/Cu–Cr films.[18] After 20 min at 200 °C, the $Cu_6Sn_5$ spheroids have departed from the bottom surface and moved towards the upper interface, assisted by gravitational force. Figure 12(a) depicts the conservative or constant volume ripening between two neighboring scallops and a large gap between them. The gap allows the molten solder to be in contact with the Cr surface, which is unwetted by the molten solder. Figure 12(b) depicts the transformation from a hemispherical-type particle to a sphere driven by lowering the sum of surface and interfacial energies in conservative ripening.

### C. No spalling in eutectic SnPb on Cu/Ni(V)/Al thin films

Due to the spalling behavior discussed above, the UBM structure of Cu/Ni(V)/Al thin films was introduced for eutectic SnPb solder bumping. Figure 13(a) shows a cross-sectional TEM image of the solder–thin film interface after one reflow, wherein the Si, $SiO_2$, a bilayer of Al, Ni(V), and $Cu_6Sn_5$ are seen.[20] Within the $Cu_6Sn_5$ layer, isolated regions of unreacted Cu surrounded by a cluster of small $Cu_3Sn$ grains were found. Between the $Cu_3Sn$ and Cu, there are Kirkendall voids. Figure 13(b) shows a cross-sectional TEM image of the interface after additional annealing of 5 min at 200 °C. Neither Kirkendall voids nor $Cu_3Sn$ grains can be observed. The $Cu_6Sn_5$ showed some grain growth but attached very well to the Ni(V). Even after 20–40 min annealing at 220 °C, very little change was found, and the $Cu_6Sn_5$ and Ni(V) layers were stable. Figure 13(c) is a higher magnification image of the Ni(V) layer and its interface with the

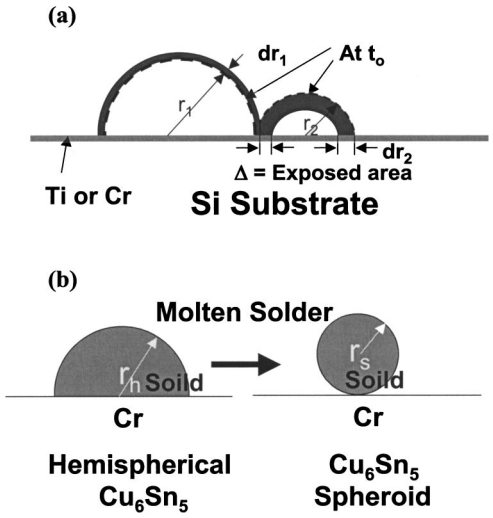


FIG. 12. Schematic diagram depicting conservative or constant volume ripening between two neighboring scallops and the opening of a large gap between them. The dotted and solid hemispheres represent scallops before and after ripening, respectively. After ripening, a gap of Δ is exposed. (b) Schematic diagram depicting the transformation from a hemispherical-type particle to a sphere driven by lowering the sum of surface and interfacial energies in conservative ripening.

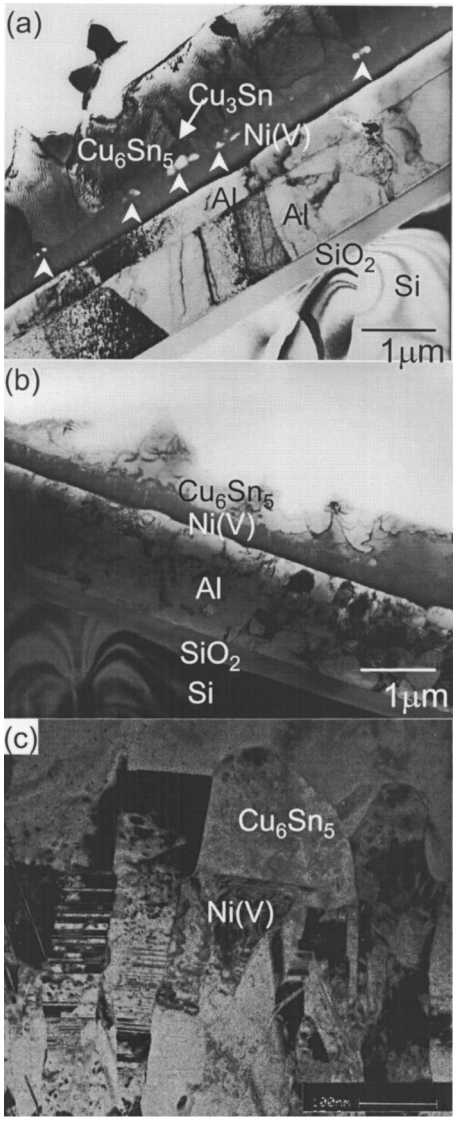


FIG. 13. (a)Cross-sectional TEM image of the interface between eutectic SnPb and Cu/Ni(V)/Al thin film metallization after one reflow, wherein the Si, $SiO_2$, a bilayer of Al, Ni(V), and $Cu_6Sn_5$ are seen. Within the $Cu_6Sn_5$ layer, isolated regions of unreacted Cu surrounded by a cluster of small $Cu_3Sn$ grains were found. Between the $Cu_3Sn$ and Cu, there are Kirkendall voids. (b) Cross-sectional TEM image of the interface after additional annealing of 5 min at 200 °C. Neither Kirkendall voids nor $Cu_3Sn$ grains are found. The $Cu_6Sn_5$ showed some grain growth but it attached very well to the Ni(V). (c) Higher magnification TEM image of the Ni(V) layer and its interface with the $Cu_6Sn_5$ layer. A large number of twin boundaries in the Ni are seen (courtesy of George T. T. Sheng ad C. H. Tung, Institute of Microelectronics, Singapore) (after Ref. 20).

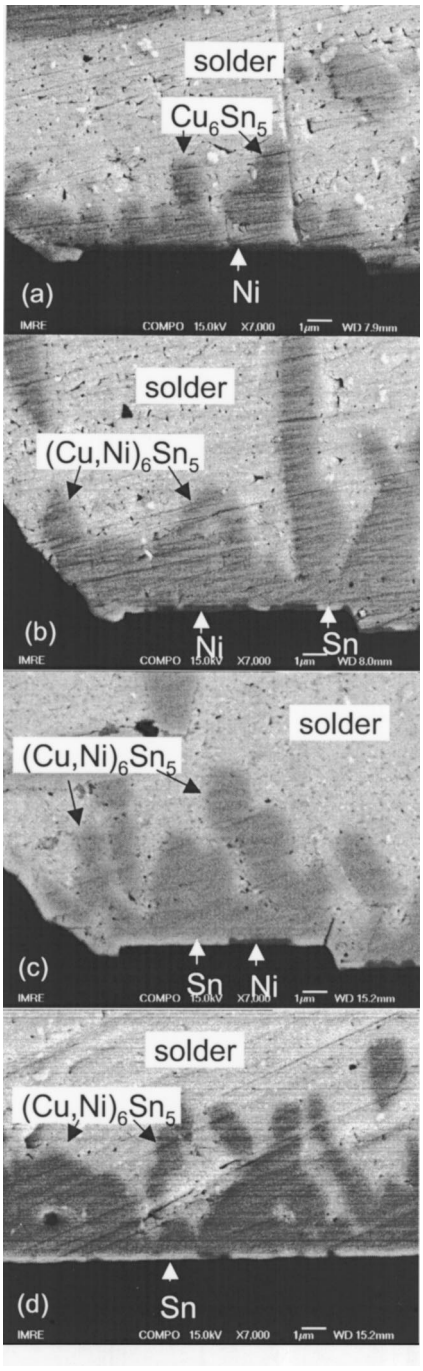


FIG. 14. SEM backscattering images at high magnification showing the evolution of the Al/Ni(V)/Cu UBM structure with the number of reflows in SnAgCu solder. (a) After 1 reflow, the Cu layer was consumed and converted to $Cu_6Sn_5$, while the Ni(V) layer was intact. (b) After 5 reflows, white patches were seen in the Ni(V) layer. The patches were confirmed by EDX as mainly containing Sn and V. (c) After 10 reflows, the white patches dominated the Ni(V) layer. (d) After 20 reflows, the Ni(V) layer disappeared and a layer of Sn separated the IMC from the Al layer. It is Sn rather than the Ni–Sn IMC that is found in place of the original Ni(V) layer (after Ref. 21).

$Cu_6Sn_5$ layer. When Ni contains more than 7 wt % V, it is diamagnetic and can be sputtered at a high rate. The V seems to have lowered the stacking fault energy of Ni, so a large number of twin boundaries in the Ni are seen in Fig. 13(c). Why does the $Cu_6Sn_5$ not transform into spheroids and spall into the solder? A plausible answer is that the interface between $Cu_6Sn_5$ and Ni(V) is a very low energy interface, hence it is stable against morphological transformation.[20]

### D. Spalling in eutectic SnAgCu solder on Cu/Ni(V)Al thin films

Since the Cu/Ni(V)/Al UBM is stable with eutectic SnPb, it has been applied to Pb-free solder.[21] Figure 14 shows SEM backscattering images of cross sections of samples of eutectic SnAgCu solder on Al/Ni(V)/Cu thin films after 1 (i.e., the as-bonded condition), 5, 10, and 20 reflows. Two types of IMC, $Cu_6Sn_5$ [also $(Cu,Ni)_6Sn_5$)] and $Ag_3Sn$, were found in the solder bump after these reflows.

The $Cu_6Sn_5$ is located mainly at the interface, although some large amounts of $Cu_6Sn_5$ also existed inside the solder.

After one reflow, the Cu layer was consumed and converted to $Cu_6Sn_5$, while the Ni(V) layer was intact as shown in Fig. 14(a). After five reflows, the morphology of the IMC changed from a rounded scallop shape to an elongated scallop or rod shape with an increase in the aspect ratio. The IMC was faceted and some of them had broken away from the UBM. Since the 300 nm Cu layer in the UBM had been consumed after one reflow (the as-bonded condition), the volume of the $Cu_6Sn_5$ IMC might not be expected to increase much during subsequent reflows. However, the cross-sectional SEM images shown in Fig. 14(b) indicate that the IMC volume does increase with the number of reflows due to the alloying of Ni in $Cu_6Sn_5$, transforming it to $(Cu,Ni)_6Sn_5$. Energy dispersive x-ray (EDX) analyses have confirmed the transformation. White patches were seen in the Ni(V) layer shown in Fig. 14(b). The patches were confirmed by EDX as mainly containing Sn and V. With the number of reflows increased to 10, the white patches dominated the Ni(V) layer as shown in Fig. 14(c). After 20 reflows, the Ni(V) layer disappeared and a layer of Sn separated the IMC from the Al layer; see Fig. 14(d). It is Sn rather than Ni–Sn IMC that is found in place of the original Ni(V) layer. Some of intermetallic rods detached from the UBM and spalled into the solder. Clearly, the UBM becomes unstable with eutectic SnAgCu after multiple reflows.

The dissolution of Ni(V) by the molten Pb-free solder is nonuniform and seems to have initiated on certain weak spots on the Ni(V) surface and spread laterally. SEM backscattering images of the eutectic SnAgCu solder on Al/Ni(V)/Cu thin films annealed at 260 °C for 5, 10, and 20 min are shown in Figs. 15(a)–15(c), respectively. The nonuniform dissolution of the Ni(V) layer and the formation of white patches in the layer increased with the amount of annealing.

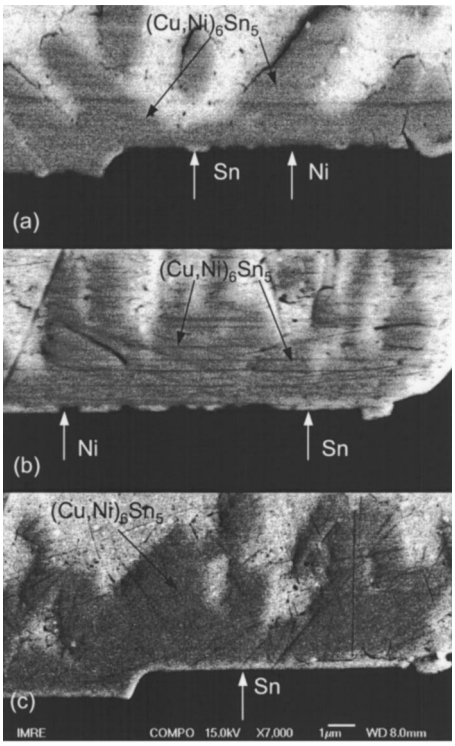


FIG. 15. SEM backscattering images at high magnification showing the evolution of the Al/Ni(V)/Cu UBM structure with the annealing time at 260 °C in molten SnAgCu solder. The annealing times were (a) 5, (b) 10, and (c) 20 min (after Ref. 21).

### E. Enhanced spalling due to interaction across a solder joint

The $(Cu,Ni)_6Sn_5$ particles from the Cu/Ni(V)/Al thin film UBM, discussed in Sec. II D, can be induced to spall quickly by interaction of the metallization on the other side of the solder joint. Figure 6 has already shown such a case. Without metallization on the other side of a solder joint, i.e., just a bump of eutectic SnCuAg on Cu/Ni(V)/Al, spalling was observed after 20 reflows. With a metallization of Au/Ni(P) joined to the other side of the bump, the spalling occurs after five reflows. Table II compares the effects on spalling with and without the interaction of metallization from the other side of a solder joint. Both SnPb and Pb-free solder joints were studied and similar results are shown in Table II.[13]

In the molten solder, the diffusivity is about $10^{-5}$ $cm^2/s$, hence it takes only 10 s for atoms to diffuse across a molten solder joint 100 $\mu$m in diameter. Since there are Au, Ni, and P on the other side of the solder joint, one of them could have enhanced the spalling. It turns out that if the Au/Ni(P) is replaced by a piece of pure Ni on the other side of the solder joint, enhanced spalling of the IMC occurs. The dissolution of pure Ni into the molten solder enhances dissolution of the $Cu_6Sn_5$ compound and exposes the Ni(V) layer to the molten solder. The enhanced dissolution of $Cu_6Sn_5$ is due to the formation of $(Cu,Ni)_6Sn_5$.

## III. MORPHOLOGICAL CHANGES OF INTERFACIAL INTERMETALLIC COMPOUNDS

As discussed in the above, spalling is a consequence of a morphological change of the IMC at an interface. In the following, we investigate the morphological changes of IMCs affected by solder composition and solid state aging.

TABLE II. Dissolution of Ni(V) thin film in Cu/Ni(V)/Al UBM after multiple reflow.

| Joint structure | Solder | Fraction of Ni(V) dissolved by molten solder |
|---|---|---|
| Solder on Cu/Ni(V)/Al | Sn–37Pb | No dissolution after 20 reflows |
| UBM (without Au) | Sn–3.5Ag–1.0Cu | 60% after 10 reflows |
| Ni(P)/Au bond pad soldered on Cu/Ni(V)/Al | Sn–37Pb | 30% after 10 reflows; 100% after 20 reflows |
| UBM (with Au) | Sn–3.5Ag–1.0Cu | 50% after 1 reflow; 100% after 3 reflows |

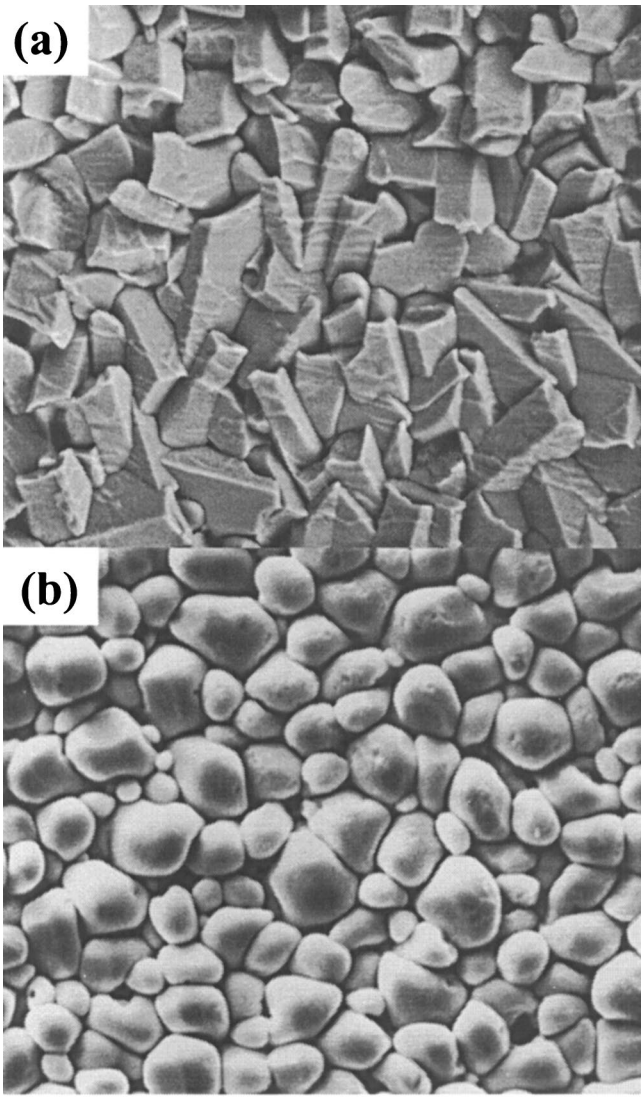


FIG. 16. (a) SEM images of the top view of the morphology of $Cu_6Sn_5$ formed between Cu and pure Sn after etching the Sn away. The $Cu_6Sn_5$ compound formed with pure Sn is highly faceted. (b) Morphology between Cu and eutectic SnPb the same compound is rounded with eutectic SnPb (courtesy of Jong-ook Suh, UCLA).

### A. Effect of solder composition on the morphology of IMCs

Figures 16(a) and 16(b) show top-view SEM images of the morphology of $Cu_6Sn_5$ formed between Cu and pure Sn and between Cu and eutectic SnPb, respectively, after etching the solder away. The interfacial compound formed is the same, yet the morphology is different. The $Cu_6Sn_5$ compound formed on pure Sn is highly faceted, but it is rounded on eutectic SnPb. Clearly this is due to the change in interfacial energy between the molten solder and $Cu_6Sn_5$; the interfacial energy is highly anisotropic with molten pure Sn. We found that if we take the scallops formed in eutectic SnPb as the reference, they become more faceted when several percent of Sn is added to the eutectic, but they become more rounded when several percent of Pb is added to the eutectic. The Pb tends to make the interfacial energy of scallops more isotropic. No high-Pb result is reviewed here since it forms a different compound of $Cu_3Sn$.

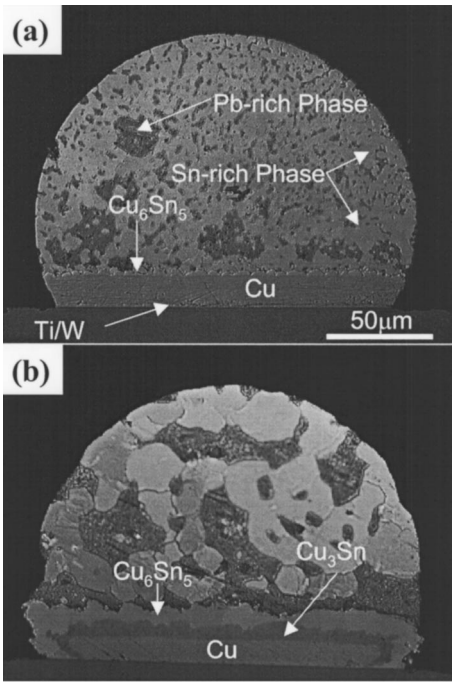


FIG. 17. (a) SEM image of an eutectic SnPb bump on a thick Cu substrate reflowed twice at 200 °C. (b) SEM image of the sample with additional aging at 170 °C for 1000 h. After aging, both $Cu_6Sn_5$ and $Cu_3Sn$ compounds show a layer-type morphology and their interfaces are rather flat. (after Ref. 25).

The effect of annealing time on the morphology of scallops between Cu and eutectic SnPb was shown in Fig. 3. In 10 min, the scallops grow big but the morphology does not change much. However, when the annealing time in molten eutectic SnPb solder was extended to tens of hours, long whiskers of $Cu_6Sn_5$ were observed.[22,23]

The effect of temperature on the morphology of scallops is small when the solder is in the molten state. Within 50 °C or so above the melting point of the solder, the change in morphology of the scallops is small. However, across the melting point of the solder, it has a dramatic change. This will be discussed below.

### B. Effect of wetting reactions and solid state aging on the morphology of IMCs

A reaction above the melting point of the solder is defined as a wetting reaction. Below the melting point, it is defined as solid state aging. The major difference between them is the amount of reaction time and the morphology of the reaction products. In the wetting reaction, it is about 1 min, yet in solid state aging, it is over hundreds of hours.[24,25] Figure 17(a) shows a SEM image of a eutectic SnPb bump on a thick Cu substrate reflowed twice at 200 °C. Figure 17(b) is an image of the sample with additional aging at 170 °C for 1000 h. After aging, both $Cu_6Sn_5$ and $Cu_3Sn$ compounds show a layer-type morphology: their interfaces are rather flat. Specifically, the $Cu_6Sn_5$ no longer shows the channels in a scallop-type morphology and the $Cu_3Sn$ is a very thick layer. Since the sample was reflowed twice before aging, it must possess scallops of $Cu_6Sn_5$ in the initial stage

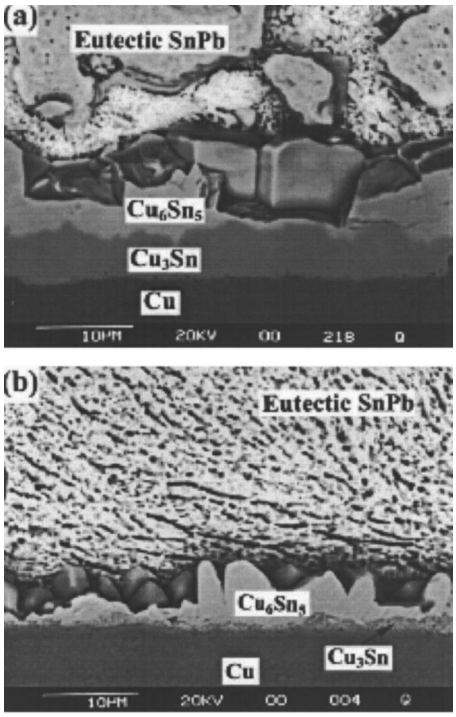


FIG. 18. (a) SEM image of the cross section of eutectic SnPb on Cu foil which was aged at 170 °C for 960 h. In the layered IMC, a few grains with vertical flat grain boundaries are seen as well as a rather thick layer of $Cu_3Sn$ that formed below the $Cu_6Sn_5$. (b) SEM image of the sample after an additional reflow at 200 °C 40 min; the $Cu_6Sn_5$ grains transformed back into scallops (after Ref. 32).

of aging, shown in Fig. 17(a). During solid state aging the morphology of $Cu_6Sn_5$ has changed from scallop type to layer type.

Interestingly, if we wet the layered IMC with molten eutectic SnPb solder again, the scallop-type morphology of $Cu_6Sn_5$ returns. Figure 18(a) shows a SEM image of the cross section of a sample of eutectic SnPb on Cu foil which was aged at 170 °C for 960 h. In the layered IMC, a few of the grains with vertical flat grain boundaries are shown, as is a rather thick layer of $Cu_3Sn$ that formed below the $Cu_6Sn_5$. When this sample was given an additional reflow at 200 °C for 40 min, the grains transformed back into scallops, as shown in Fig. 18(b). We found that only 1 min at 200 °C is enough to transform layer-type $Cu_6Sn_5$ back to scallop-type $Cu_6Sn_5$. The results in Fig. 18 show that scallop-type grains are stable when in contact with molten solder, but the layer-type grains are stable when in contact with solid solder.

The stability is due to minimization of interfacial and grain boundary energies. The interfacial energy between a molten solder and $Cu_6Sn_5$ is less than that between a solid solder and $Cu_6Sn_5$, so the scallop-type morphology of grains persists in wetting reactions and the layer-type morphology persists in solid state aging. When the molten solder reacts with the layer-type $Cu_6Sn_5$ and transforms it back into scallop-type $Cu_6Sn_5$, the reaction begins by wetting the large angle grain boundaries in the layer-type $Cu_6Sn_5$, as depicted in Fig. 19. This implies that the energy of the interface between solid solder and $Cu_6Sn_5$ ($\sigma_{SS}$) as well as the energy of large angle grain boundaries in $Cu_6Sn_5$ ($\sigma_{GB}$)

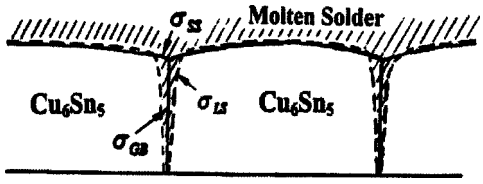


FIG. 19. Schematic diagram depicting the reaction between molten solder and the layer-type $Cu_6Sn_5$ and the transformation of the layer-type $Cu_6Sn_5$ back into scallop type. The reaction begins by wetting the large angle grain boundaries in the layer-type $Cu_6Sn_5$.

must be quite high, so they can be replaced by the low energy interfaces of the molten solder and $Cu_6Sn_5$ ($\sigma_{SL}$).

During wetting reactions, the neighboring scallops will not join together and form grain boundaries. Therefore they can only grow bigger (sidewise) by ripening or they have to grow in height. The sidewise growth is parasitic. On the other hand, the scallops cannot keep on growing sidewise and become very big. This is because the bigger the scallops, the lesser the channels per unit area of the interface. Since channels are the short circuit paths for Cu atoms to reach the molten solder, scallop-type growth will slow down when the number of channels is reduced. Indeed, over very long annealing times in molten eutectic SnPb solder on Cu, the Cu6Sn5 has grown into whiskers rather than big scallops.[22,23]

The activation energy of the wetting reaction was found to be about 0.2–0.3 eV/atom.[15] This is comparable to the activation energy of dissolution of Cu into Sn in the reaction between Cu and molten Sn, i.e., 0.18 eV in the range of 240–280 °C.[26] The wetting reaction is a very low activation energy process. On the other hand, in solid state aging of eutectic SnPb on Cu, the activation energy of the growth of layer-type $Cu_6Sn_5$, or $Cu_3Sn$ (or the total thickness of the two layers), is about 1 eV/atom.[25] So solid state aging is a much slower kinetic process. A direct way to compare the wetting reaction and solid state aging is to compare the period of time needed to form the same amount of IMC. In a wetting reaction at 200 °C, it takes only a few minutes to form a few microns of $Cu_6Sn_5$, but in solid state aging at 170 °C, it takes 1000 h to do so. So the wetting reaction is four orders of magnitude (in terms of time) faster than solid state aging, although the difference in temperature between 200 and 170 °C is only 30 °C. Table III lists the differences between these two reactions.[24]

We can look at the difference from another angle. Atomic diffusivity in the liquid state is about $10^{-5}$ $cm^2/s$, and the diffusivity in a face-centered-cubic metal near its melting point is about $10^{-8}$ $cm^2/s$. Across the melting point

TABLE III. A comparison between the solder wetting reaction and solid state aging.

| Solder reaction | Wetting reaction | Solid state aging |
|---|---|---|
| Temperature and time | 200 °C, 2 min | 170 °C, 1500 h (90 000 min) |
| Morphology | Scallop-type IMC | Layer-type IMC |
| Growth velocity | $v=1$ μm/min | $v=10^{-4}$ μm/min |
| Activation enthalpy | $\Delta H=0.2$–$0.3$ eV | $\Delta H=1.0$–$1.1$ eV |

there is a difference of three orders of magnitude in diffusivity. Thus, if we perform the wetting reaction a few degrees above the melting point and solid state aging a few degrees below the melting point, we will find a similar difference in their reaction rates. This difference in diffusivity is in agreement with the difference in time found in the reactions to form the same amount of IMC on the basis of the diffusion relation of $x^2 \approx Dt$.

Knowing the activation energy of 1 eV/atom of solid state reaction, we ask, if the growth of the $Cu_6Sn_5$ compound during the wetting reaction at 200 °C assumes a layer-type morphology, what would happen? Consider the formation of a layer of 1 $\mu$m thick $Cu_6Sn_5$ by consuming about 0.5 $\mu$m of Cu. It would have taken more than 1000 s for Cu atoms to diffuse through such a $Cu_6Sn_5$ layer, so it becomes a diffusion barrier and the rate of reaction becomes very slow. On the other hand, it actually takes less than 1 min to consume 0.5 $\mu$m of Cu and form $Cu_6Sn_5$ scallops in a wetting reaction.[27] In other words, the rate of free energy gain will be much faster in scallop-type growth than in layer-type growth. Therefore, it is the rate of change of free energy, rather than the change of free energy itself which determines scallop-type IMC growth. The morphology of the reaction product in the form of scallops has enabled a high rate of reaction to take place in wetting reactions. The radius of the scallop cannot remain constant because it must grow bigger over time, so ripening occurs. What the distribution of the size of scallops is an important question in kinetic analysis. Whether the distribution function is time dependent and whether it is the same function given by classic Lifshitz–Slezov–Wagner (LSW) theory of ripening[28–30] will be analyzed in Sec. IV.

## IV. KINETIC THEORY OF RIPENING OF INTERFACIAL INTERMETALLIC COMPOUNDS

### A. Ripening under constant surface and increasing volume

Figure 20(a) shows a schematic diagram of the cross section of an array of hemispherical $Cu_6Sn_5$ scallops grown on Cu, shown by the solid curves. The following assumptions are made to analyze the kinetics of scallop growth.[31] (a) The presence of $Cu_3Sn$ and Pb in the reaction is ignored for convenience. (b) A liquid channel exists between two scallops, the depth of which reaches the Cu surface. The width of the channel $\delta$ is assumed to be small compared to the radius of the scallops. The morphology of scallops and channels is assumed to be thermodynamically stable in the presence of molten solder.[32,33] The channels serve as rapid diffusion paths for Cu to go into the molten solder to grow the scallops. Although the scallops are separated by channels, they remain in close contact with each other; see Fig. 16(b). Figure 20(b) is a cross-sectional transmission electron microscopic image of $Cu_6Sn_5$ scallops, channels, and a thin layer of $Cu_3Sn$ on Cu. The channel, indicated by an arrow, has width less than 50 nm. (c) For simple mathematical analysis, the geometrical shape of the scallops is represented by the hemisphere. On a given interfacial area of $S^{\text{total}}$ between the scallops and the Cu, the total surface area between all hemispherical scallops and molten solder is just twice $S^{\text{total}}$. In

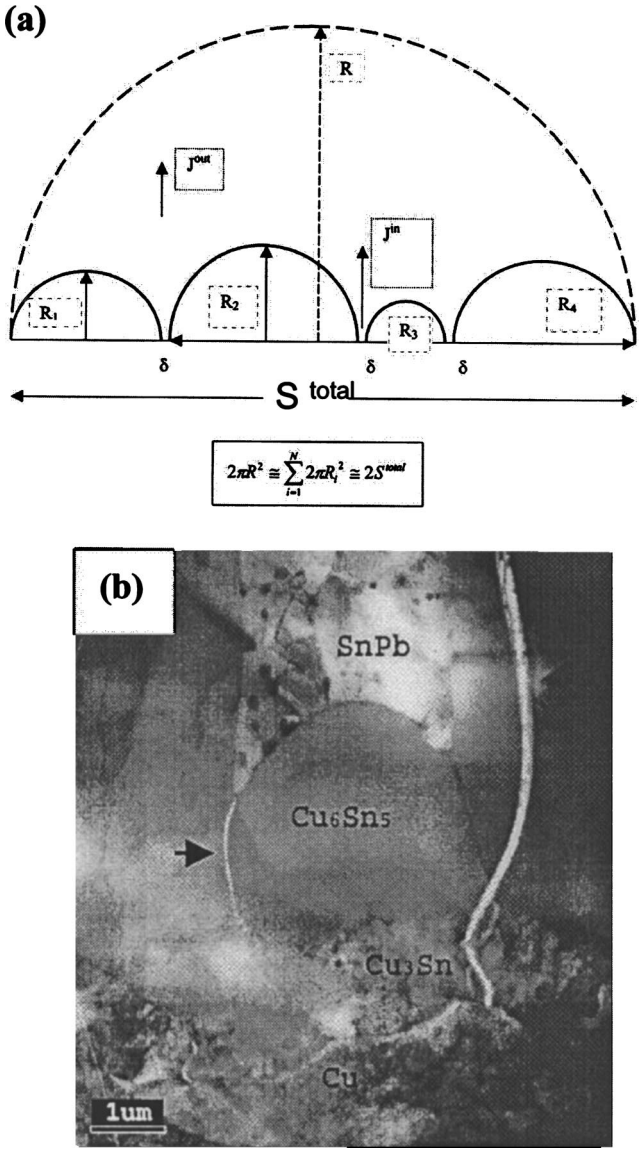


FIG. 20. (a) Schematic diagram of the cross section of an array of hemispherical $Cu_6Sn_5$ scallops grown on Cu, represented by the solid curves. (b) Cross-sectional TEM image of $Cu_6Sn_5$ scallops, channels, and a thin layer of $Cu_3Sn$ on Cu. The channel, indicated by an arrow, has width of less than 50 nm (courtesy of George T. T. Sheng, MXIC, Hsinchu, Taiwan, ROC) (after Ref. 31).

Fig. 20(a), if we represent the cross section of a large hemispherical scallop by the broken half circle, its surface is $2S^{\text{total}}$, the same as the sum of the surfaces of the smaller scallops represented by solid curves. Hence, while growth increases the total volume, it does not change the total surface area of the scallops. (d) By conservation of mass, we assume that all influx of Cu from the Cu substrate is consumed by the growth of scallops. Hence, the outflux of Cu from the ripening zone into the bulk of the molten solder is assumed to be negligible.

Since growth of a scallop must occur at the expense of its neighbors, it is a ripening process. In this ripening process, there are two important constraints. The first constraint is that the interface of reaction is constant. When the scallops are assumed to be hemispherical, it also means that the total surface area of scallops is constant. Therefore we have a

ripening process which proceeds under a constant surface with increasing volume. The second constraint is conservation of mass, in which all the influx of Cu is consumed by scallop growth. It is different from classical ripening, in which the process proceeds under an almost constant volume, so the decrease of surface (and surface energy) provides the driving force.

Let $f(t,R)$ be the size distribution function of scallops, so that the total number of scallops is equal to

$$N(t)=\int_0^\infty f(t,R)dR, \tag{1}$$

and the average values are

$$\langle R^m\rangle=\frac{1}{N}\int_0^\infty R^m f(t,R)dR. \tag{2}$$

The first constraint of the constant interface takes the form of

$$\int_0^\infty \pi R^2 f(t,R)dR=S^{\text{total}}-S^{\text{free}}\cong S^{\text{total}}=\text{const.} \tag{3}$$

The cross-sectional area of all channels for copper supply is

$$S^{\text{free}}=\int_0^\infty \frac{\delta}{2}2\pi R f(t,R)dR. \tag{4}$$

The total volume of the growing scallops is

$$V_i=\int_0^\infty \frac{2}{3}\pi R^3 f(t,R)dR. \tag{5}$$

According to the second constraint, we have

$$n_i C_i\frac{dV_i}{dt}=J^{\text{in}}S^{\text{free}}. \tag{6}$$

Here $n_i$ is the atomic density in the IMC, i.e., the number of atoms per unit volume, and $C_i$ is the atomic fraction of Cu in the IMC, which is 6/11 in $Cu_6Sn_5$. The influx is taken approximately as

$$J^{\text{in}}=-nD\frac{[C^e+(\alpha/R)]-C^b}{R}, \tag{7}$$

where $n$ is the atomic density in solder, $\alpha=(2\gamma\Omega/k_GT)C^e$, $\gamma$ is isotropic surface tension at the IMC/melt interface, $\Omega$ is the molar volume, $k_G$ is Boltzmann constant, and $T$ is the temperature. $C^e$ and $C^b$ are defined as the equilibrium concentration (the atomic fraction of Cu in molten solder) on a flat surface and the concentration at the entrance of the channels (corresponding to the concentration of Cu in the molten solder on the substrate surface), respectively.

Since scallops must grow and shrink atom by atom, the distribution function should satisfy the usual continuity equation in size space:

$$\frac{\partial f}{\partial t}=-\frac{\partial}{\partial R}(fu_R), \tag{8}$$

where the velocity in size space, $u_R$, is simply the growth rate of scallops with radius $R$ and is determined by the flux density, $j(R)$, on each individual scallop. The expression for $j(R)$ is usually found to be a quasistationary solution of the diffusion problem in infinite space around a spherical grain with fixed supersaturation $\langle C\rangle-C^e$ at infinity. Then

$$u_R=\frac{dR}{dt}=-\frac{j(R)}{n_iC_i}=\frac{n}{n_i}\frac{D}{C_i}\frac{\langle C\rangle-(C^e+\alpha/R)}{R}. \tag{9}$$

While this expression is good for LSW theory, it is not good for the present case because the scallops are on an interface and the distance between them is of the same order of magnitude as the size of scallops. On the other hand, diffusion in the melt is very fast, so we suggest that the expression of $j(R)$ can be obtained by assuming that the flux on (or out of) each individual scallop should be proportional to the difference between the average chemical potential of copper $\mu$ in the reaction zone (we take it to be the same everywhere, the mean-field approximation) and the chemical potential at the curved scallop–melt interface, $\mu_\infty+\beta/R$, and $\beta=2\gamma\Omega$:

$$-j(R)=L\left(\mu-\mu_\infty-\frac{\beta}{R}\right),\ \frac{dR}{dt}=\frac{L}{n_iC_i}\left(\mu-\mu_\infty-\frac{\beta}{R}\right), \tag{10}$$

where the parameters $L\beta,\mu-\mu_\infty$ are determined self-consistently from the above mentioned two constraints of the constant surface, Eq. (3), and mass conservation, Eq. (6). We obtain

$$u_R=\frac{dR}{dt}=\frac{k}{9}\frac{1}{\langle R^2\rangle-\langle R\rangle^2}\left(1-\frac{\langle R\rangle}{R}\right), \tag{11}$$

$$k=\frac{9}{2}\frac{n}{n_iC_i}D(C^b-C^e)\delta. \tag{12}$$

During nonconservative flux-driven ripening, the rate of growth/shrinkage of each scallop is determined not only by diffusivity and the average size of all scallops, $\langle R\rangle$, but also by the capacity of channels to supply Cu for the reaction.

Thus in the mean-field approximation, the basic equation for the distribution function has the following form:

$$\frac{\partial f}{\partial t}=-\frac{k}{9}\frac{\langle R\rangle}{\langle R^2\rangle-\langle R\rangle^2}\frac{\partial}{\partial R}\left[f\left(\frac{1}{\langle R\rangle}-\frac{1}{R}\right)\right], \tag{13}$$

where the rate coefficient $k$ is determined by the incoming flux conditions, which in turn are determined by the channels.

The formal solution of our distribution function is

$$f(t,R)=\frac{B}{bt}\frac{R}{(bt)^{1/3}}\exp\left\{\int_0^{R/(bt)^{1/3}}\frac{3-4\xi}{\xi^2-3\xi+9/4}d\xi\right\}$$

$$=\frac{B}{\tau}\varphi(\eta),\tau=bt,\eta=\frac{R}{(bt)^{1/3}}, \tag{14}$$

$$B=\frac{S^{\text{total}}}{\pi\int_0^\infty \xi^2\varphi(\eta)d\eta}. \tag{15}$$

The parameter $b$ should be found self-consistently.

Standard integration gives

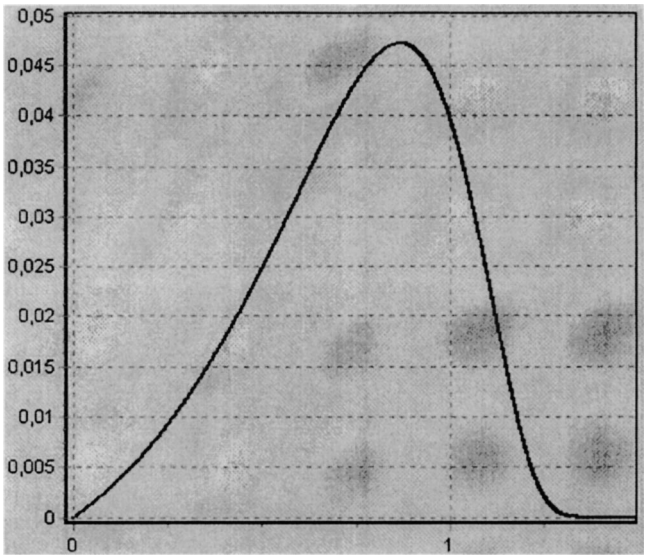


FIG. 21. Plot of the asymptotic size distribution function.

$$\varphi(\eta)=0, \eta>\left(\frac{3}{2}\right),$$

$$\varphi(\eta)=\frac{\eta}{\left(\frac{3}{2}-\eta\right)^4}\exp\left(-\frac{3}{\frac{3}{2}-\eta}\right), \quad 0<\eta<\left(\frac{3}{2}\right). \quad (16)$$

The plot of $\varphi(\eta)$ vs $\eta$ is shown in Fig. 21. Thus, we have a unique asymptotical solution which satisfies the universal scaling expression in Eq. (15). Also, we have

$$\langle\eta^2\rangle-\langle\eta\rangle^2\cong 0.0615, \langle\eta\rangle=3/4, \langle\eta^3\rangle\cong 0.5535.$$

Parameter

$$b=\frac{k}{9(\langle\eta^2\rangle-\langle\eta\rangle^2)}\cong\frac{k}{0.5535}\cong\frac{k}{\langle\eta^3\rangle}.$$

Hence, the average cube of the grain size is equal to

$$\langle R^3\rangle=\langle\xi^3\rangle bt\cong kt.$$

The average size will be

$$\langle R\rangle=\langle\xi\rangle(bt)^{1/3}\cong\frac{3}{4}\left(\frac{k}{0.5535}t\right)^{1/3}\cong 0.913(kt)^{1/3}.$$

If we take $n/n_i\approx 1$, $C_i=6/11$, $D\approx 10^{-5}$ cm$^2$/s, $\delta\approx 5\times 10^{-6}$ cm, $C^b-C^e\approx 0.001$, where the concentration $C^b$ is taken for equilibrium of the melt with the $Cu_3Sn_1$ phase, the rate constant $k\approx 4\times 10^{-13}$ cm$^3$/s. For example, for annealing time $t=300$s, it gives $R\approx 5\times 10^{-4}$ cm, which agrees very well with the experimental data. The rate of ripening and growth of $R$ is determined by the incoming flux condition.

## V. PHYSICS CHALLENGES

### A. Calculation of surface and interfacial energies

The rate of the solder reaction should depend on the thermodynamic driving force and kinetics. It seems that, as discussed in Sec. III, it also depends on morphology. The ternary phase diagrams of Sn–Pb–Cu at 200 and 170 °C, shown in Fig. 10, are not much different from the point of view of phase formation. Both the reactions at 200 and 170 °C lead to formation of $Cu_6Sn_5$ and $Cu_3Sn$. The formation energy of the IMC at these two temperatures is nearly the same since its dependence on the temperature is small, yet the reaction rates are different by four orders of magnitude. While the difference can be explained by the difference in atomic diffusivity between the molten state and solid state, it is the morphology that dictates the kinetic path. In order to understand why in a wetting reaction, the IMC has scallop-type morphology and why in solid state aging, it changes to layered-type morphology, we need to calculate the surface and interfacial energies in these reactions. No doubt, the calculation and measurement of many surface and interfacial energies have been performed, e.g., in adhesion studies, yet we need to consider ternary systems here. Besides, in molten solder alloys, we must take into account the effect of surface segregation on the surface energy. Due to fast atomic diffusion, solute or solvent atoms can segregate to the surface of a molten solder rapidly. It was reported that the measured surface energies of molten Pb and Pb–Sn alloys up to about 20 at. % of Sn are essentially the same.[34,35] How to calculate these surface energies and solder/IMC interfacial energies is challenging.

### B. Unstable wetting tip

The classic Young's equation of an equilibrium wetting tip was derived by minimizing the total surface and interfacial energies involved, and no free energy of formation of the interfacial IMC was included.[36,37] The wetting angle is defined by the equilibrium condition among the surface and interfacial energies at the wetting tip. Assuming that the wetting tip (or a wetting cap) configuration is achieved instantaneously, the free energy of IMC formation may be ignored if the rate to form the interfacial IMC is much slower than the spreading rate for a drop of molten solder on a metal surface.

Here we shall present two phenomena in solder reactions wherein the wetting tip is unstable. The first one is the wetting of molten SnPb on Pd and Au. They show no stable wetting angle. In the case of eutectic SnPb on Pd, the tip advances on the Pd surface unceasingly until the solder is consumed entirely.[38] In the case of 95Pb5Sn solder on Au, the molten solder has an interface that sinks into Au which deepens over time.[39] In both cases, the wetting angle and the tip configuration change over time. It is because of the rapid reaction that forms the IMC in the SnPb/Pd case, and it is because of rapid dissolution of Au into the molten solder in the SnPb/Au case.[40] The other one concerns the wetting of a molten eutectic SnPb cap on Cu. While there is a stable wetting angle, the tip is unstable in the sense that it grows a halo. The halo spreads out unceasingly due to the formation of a very thin layer of IMC below the halo. The halo has also been found in front of a molten tip of eutectic SnPb on Ni.

To study the effect of IMC formation on a reactive wetting tip, we must study the very early stages of the wetting reaction. Using a lithographic technique, etched V grooves along [110] directions on (001) surfaces of Si coated with a

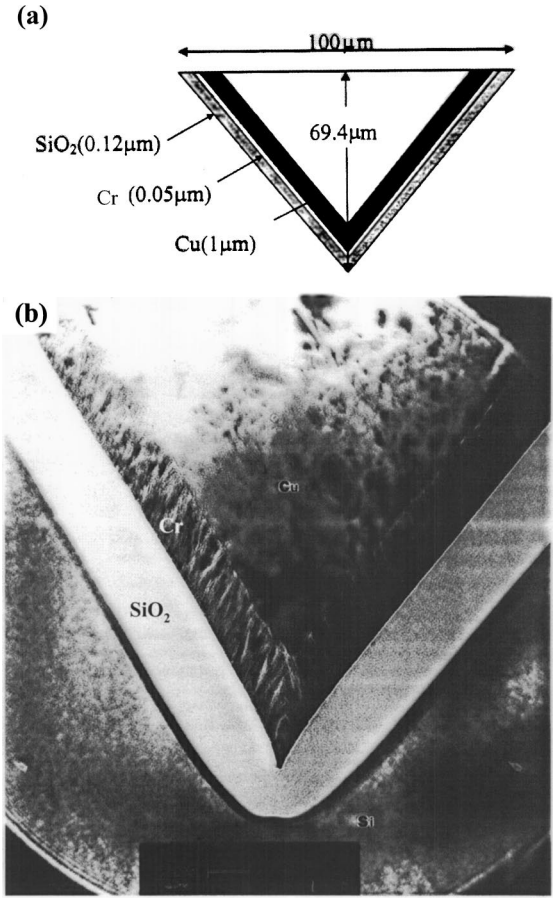


FIG. 22. (a)Schematic diagram of the cross section of a V-groove and (b) cross-sectional TEM image of a V groove (courtesy of N. Wang, Department of Physics, Hong Kong University of Science and Technology, Hong Kong) (after Ref. 55).

bilayer of Cu/Cr film were made. A schematic diagram of the cross section of a V groove and a corresponding TEM image are shown in Figs. 22(a) and 22(b), respectively. Molten pure Pb will not run into the V groove, but molten Pb(Sn) alloys having only 1%–5% of Sn will run into it because of being driven by the horizontal capillary force, as shown in the lower part of Fig. 23. The more Sn in the molten solder, the longer the length of the run (or the faster the run). The length of the run shows a direct correspondence to the wetting angle of Cu as a function of the Sn concentration in the molten solder; see the SEM images shown in the upper part of Fig. 23. While pure Pb unwets Cu, the Pb(Sn) alloy wets Cu and the wetting angle decreases with increasing amount of Sn in Pb.[41] Since the addition of a few percent of Sn does not change the surface energy of the molten solder,[34,35] no change in wetting angle is expected on the basis of Young's equation. Hence, the change is due to Cu–Sn interfacial reaction in forming the IMC. How to calculate the change in wetting angle and in turn the wetting rate as a function of the solder composition shown in Fig. 23 is challenging. The wetting rate has been given by the Washburn equation and can be measured using a charge coupled devise (CCD) camera.[42–44] Knowing the rate, it is possible to estimate the rate of IMC formation in a very early stage of the wetting reaction.

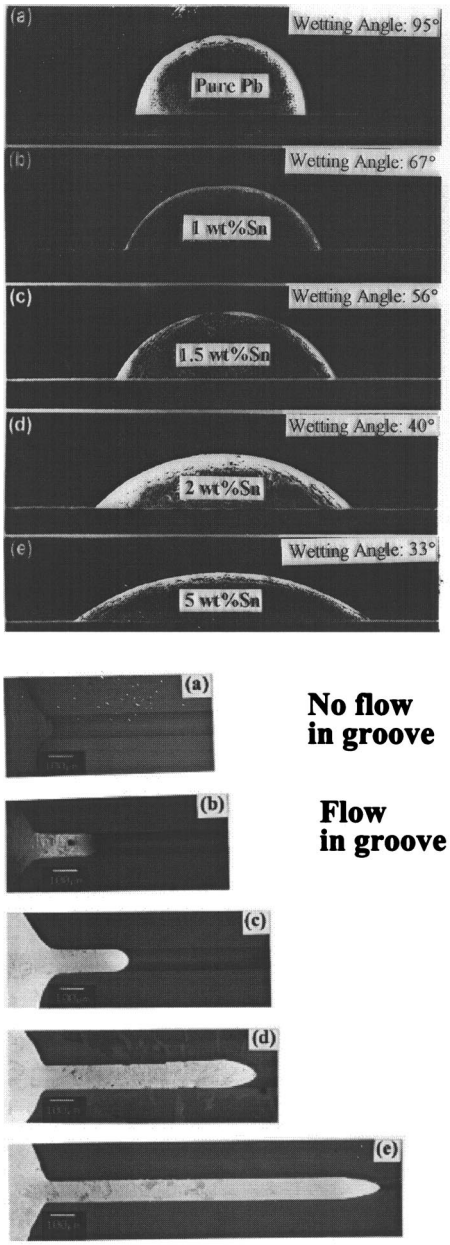


FIG. 23. Five SEM images in the upper part that show a side view of SnPb solders on the Cu surface, illustrating the decrease of the wetting angle with an increase of Sn in Pb. The five SEM images in the lower part show, correspondingly, the run of the solders in the V grooves with an increase of Sn in Pb. Molten pure Pb will not run into the V groove, but molten Pb(Sn) alloys having only 1%–5% of Sn will. The more Sn in the molten solder, the longer the length of the run (or the faster the run) (after Ref. 41).

### C. *In situ* study of molten solder–metal interfaces and reactions

The atomic model of molten solder interfaces is of interest. The interface between molten solder, say, eutectic SnPb, and Cu at 200 °C is unstable due to IMC formation. The interface between molten eutectic SnPb and $Cu_6Sn_5$ at 200 °C or that between high-Pb solder and $Cu_3Sn$ are also unstable due to the growth of the IMC, nevertheless *in situ* study of these solder/IMC interfaces by synchrotron radiation or other means is of interest. The very early stages of reaction, i.e., nucleation of the IMC on Cu and growth of the IMC before ripening, are also of interest.

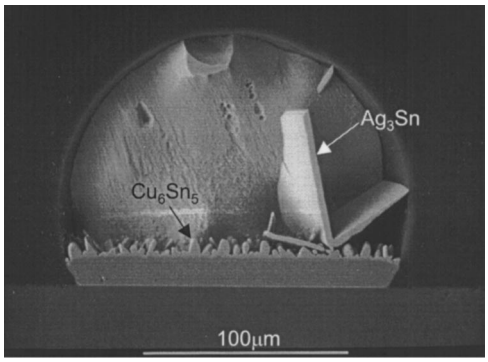


FIG. 24. SEM image of a large $Ag_3Sn$ plate-type precipitate in the eutectic SnAg solder (after Ref. 8).

## VI. MATERIALS CHALLENGES

### A. Microstructure-properties relations of Pb-free solders

In Sec. I, we discussed the eutectic solders of Sn and noble metals. Their microstructure is a mixture of Sn and IMC, unlike that of eutectic SnPb which has no IMC. The mechanical properties of these Pb-free eutectic solders will be anisotropic when dispersion of the IMC in Sn is inhomogeneous. In the case of Au–Sn, the formation of $AuSn_4$ means that one Au atom will attract four Sn atoms. Hence, a small amount of Au can lead to a large amount of IMC formation. This is the origin of a brittle ''cold'' joint when a solder joint contains more than 5 wt % Au.[45–47] In the cases of eutectic SnAg and eutectic SnAgCu, the $Ag_3Sn$ precipitates are plate like, as shown in Fig. 24. If such a $Ag_3Sn$ crystal has formed in a stress concentration region, e.g., the corner region between a solder bump and under-bump metallization, cracks can initiate and can propagate along the interface between the $Ag_3Sn$ and the solder. In the case of eutectic SnCu, it has only 0.7 wt % of Cu, so the bulk of the solder is Sn. Then, the phenomena of Sn whisker,[48–53] Sn pest,[54] and Sn cry are of concern. In addition, how to control the solder composition, say, to within $\pm 0.5$ wt % of the eutectic SnCu composition, is also quite challenging when the method of production is electroplating.

### B. Effects of irreversible processes on solder joint reliability

The reliability of the solder joints in flip chip technology can be challenged by multiple forces. The very large difference in coefficients of thermal expansion between the Si chip and the organic substrate is a concern because of thermal-mechanical stress. Due to the small size of the solder bump, electromigration is also a concern because of the high current density and the very fast atomic diffusivity at ambient temperature in the solder alloy.[55,56] We have already discussed chemical reactions between the solder and thin film UBM in Sec. II. Then temperature gradients due to local Joule heating cannot be ignored. It is interesting to point out that in the classic Soret effect,[57] a homogeneous alloy becomes inhomogeneous (dealloying) under a temperature gradient. Hence, the solder joint has a complicated reliability nature due to combined forces that are chemical, mechanical, electrical, and thermal in nature. We shall briefly discuss thermal stress and electromigration here.

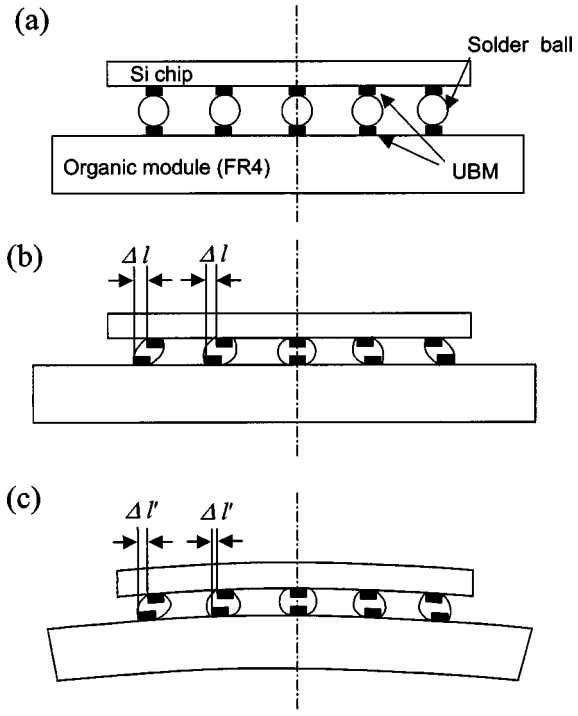


FIG. 25. Schematic diagrams illustrating the large thermal stress in flip chip on organic substrates. (a) Before solder joining. (b) When the solder is in the molten state, there is no thermal stress although the board has expanded much more than the chip. (c) Upon cooling to the solidification temperature of the solder, when the solder solidifies, thermal mismatch begins to interfere. If we assume the chip is rigid, the board will bend and the curvature is downwardly concave.

### C. Thermal stress

The thermal stress in flip chip on organic substrates is very large, as shown in Fig. 25(a), due to the very large difference in coefficients of thermal expansion between Si ($\alpha = 2.6$ ppm/C) and an organic FR4 board ($\alpha = 18$ ppm/C).[58] When the solder is in the molten state [see Fig. 25(b)], there is no thermal stress although the board has expanded much more than the chip. But upon cooling, when the solder solidifies, thermal mismatch begins to interfere. We shall take the difference in temperature to be that between room temperature and 183 °C, the solidification temperature of eutectic SnPb solder. And we consider a bump at the corner of a 1 cm$\times$1 cm chip. The shear is equal to $\Delta l/l = \Delta\alpha\Delta T$. We obtain a value of $\Delta l = 18$ $\mu$m if we take $l = (\sqrt{2})/2$ cm, which is the distance of half the diagonal of the chip. If we assume the chip to be rigid, the board will bend and the curvature will be downwardly concave. This is because the solid bumps will prevent the upper surface of the board from shrinking, so the board will bend when its lower part shrinks; see Fig. 25(c).

Due to the bending and the fact that the solder joints and the chip are not rigid, the actual $\Delta l$ will be less than the calculated value of 18 $\mu$m given in the last paragraph. Figure

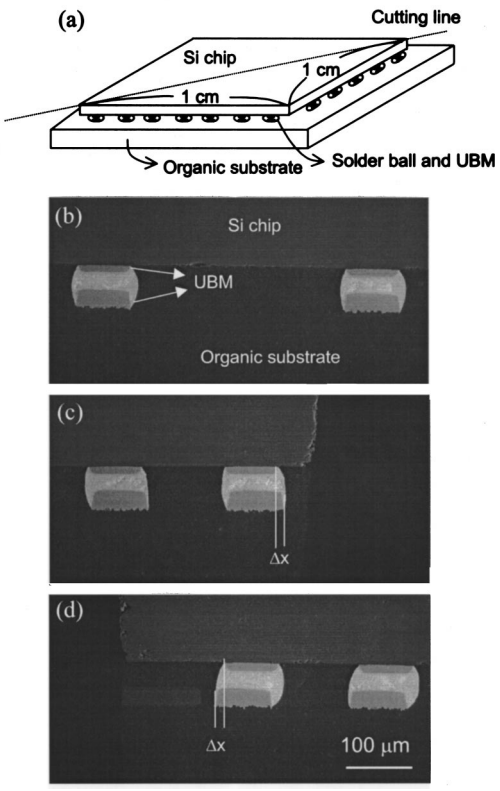


FIG. 26. (a)Schematic diagram of eutectic SnPb solder bumps between a flip chip and a FR4 board. (b) Cross-sectional SEM images of a solder joint in the center part of the chip, where the alignment between the top UBM on the chip and the bottom bond-pad on the board is good. (c) A joint at the right-hand side corner of the chip, where the bottom bond pad on the board has been displaced to the right by about 10 $\mu$m, relative to the upper UBM on the chip. (d) A joint at the left-hand side corner of the chip, with the same displacement of the bond pad but to the left (after Ref. 58).

26(a) shows a schematic diagram and cross-sectional SEM images of eutectic SnPb solder bumps between a flip chip and a FR4 board.[58] Figure 26(b) shows a joint in the center part of the chip, where the alignment between the top UBM on the chip and the bottom bond pad on the board is good. Figure 26(c) shows a joint at the right-hand side corner of the chip, where we see that the bottom bond pad on the board has been displaced to the right by about 10 $\mu$m relative to the upper UBM on the chip. Figure 26(d) shows a joint at the left-hand side corner of the chip, and the same displacement of the bond pad is to the left. The nominal shear strain is $\Delta l/h = 10/60$, where $h = 60$ $\mu$m is the gap between the chip and the board. However, the shear in the solder bump is $\Delta l/h' = 10/30$, where $h' = 30$ $\mu$m is the thickness of the solder between the UBM and the bond pad. In addition, we found that the chip is bent and has a downwardly concave curvature of 57 cm. Clearly, the chip, the board, and the bumps are stressed. Besides the shear strain, there is normal strain in the solder joint. The stress or strain distribution in a solder joint has been investigated using moiré fringes.[59–61] We can also use microdiffraction in synchrotron radiation to map the strain distribution. The high intensity x-ray beam can be focused to less than 1 $\mu$m in diameter, and it can be scanned over the entire cross section of a solder joint as shown in Fig. 26. The measured strain distribution can be correlated to the grain orientation and various phases in the solder joint.

The electronic industry has introduced epoxy underfill between the chip and the board to redistribute thermal stress,[2] nevertheless it remains a reliability issue. In a multichip module with underfill, how to repair a defective chip on the module remains unresolved. If we introduce underfill in the configuration shown in Fig. 25(c), the solder joints have already been strained. Hence, it is better to apply underfill to unstrained solder joints. Assuming it can be done, e.g., we can use a laser to heat each of the solder joints locally, one by one, then the thermal stress in the joint at the corner should be much less. However, we still cannot avoid the problem of thermal stress. This is because in subsequent reflows, solid state aging, and device operation the stress comes back. During normal device operation, where the chip will experience temperature near 80–100 °C due to Joule heating, it produces low cycle thermal stress and causes fatigue of the solder joints. If the joint or one of its interfaces is mechanically weak, stress can break it. We note that it is this large shear strain shown in Fig. 26 which limits the size of a Si chip in flip chip manufacturing. Unless we can solve the thermal stress problem, the chip size will be limited to about 1–2 cm$^2$.

### D. Electromigration

For electromigration, the design rule is to distribute 1 A over five solder bumps, or 0.2 A/bump. For a solder bump 50 $\mu$m in diameter, the current density will be about $3 \times 10^3$ A/cm$^2$. Since the contact area of the bump is much smaller than the cross section of the bump, the actual current density will reach about $10^4$ A/cm$^2$ at the solder bump contact. While this current density is about one order of magnitude less than that in Al or Cu interconnects,[62–71] electromigration in a solder bump is a reliability concern, and it is different from that in Al or Cu interconnects for the following reasons. First, because of the low melting point and high atomic diffusivity of solder alloys, the rate of electromigration is fast even near room temperature. Second, because of the line-to-bump configuration, a large change in current density occurs when the current enters the solder bump from the interconnect line (or vice versa), resulting in current crowding at the contact between them.[72] Third, because solders are eutectic alloys, there is no chemical potential gradient as a function of composition below the eutectic temperature. Hence, electromigration can induce a very large compositional redistribution in a eutectic solder joint without opposition. Fourth, because noble and near-noble metals are fast diffusers in solder alloys and they are used as UBMs in solder joints, their combination allows a rapid dissolution of UBM from the cathode side and extensive formation of IMCs at the anode side. For Sn-based solders, since the IMC is the eutectic partner of Sn, a very large amount of IMC can be formed at the anode side of the solder joint when a thick UBM of noble or near-noble metal at the cathode side is dissolved.

Experimentally, a substantial amount of electromigration has been found in eutectic SnPb solder bumps powered by a

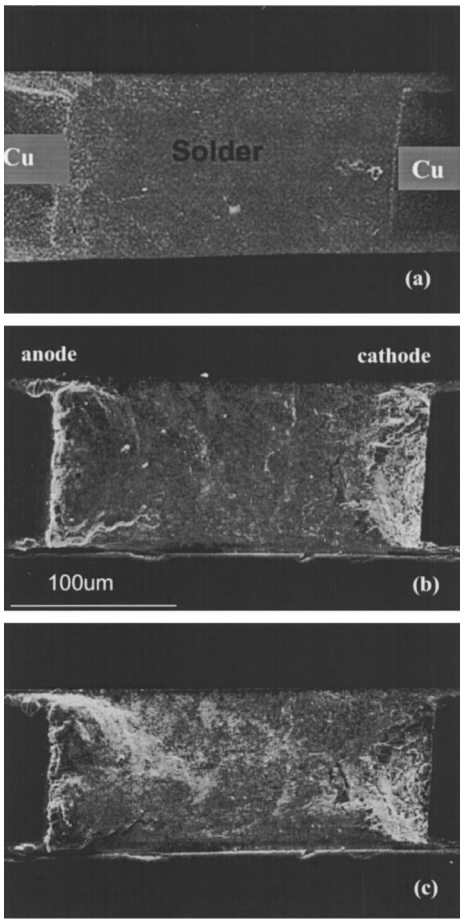


FIG. 27. (a) SEM image of a solder line in a V groove, approximately 200 $\mu$m long, 100 $\mu$m wide, and around 67 $\mu$m deep. The lines were stressed at current density of $5\times10$ A/cm$^2$ at room temperature. (b), (c) SEM images of hump and void growth in the line after being stressed for 192 and 288 h, respectively (after Ref. 56).

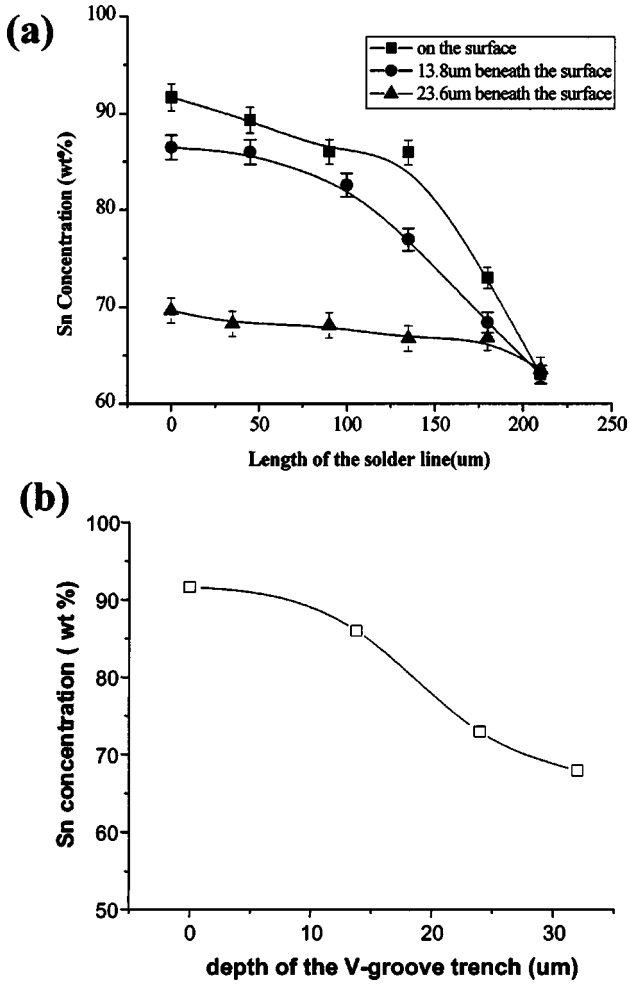


FIG. 28. (a) Compositional analysis of Sn along the solder line performed by EDX spots on the surface as well as on the polished surfaces, which were about 14 and 24 $\mu$m below the original surface. (b) The change in Sn concentration in the vertical direction, near the anode side (after Ref. 56).

current density of $8\times10^3$ A/cm$^2$ after a few hundred hours at 150°C. [73,74] At the cathode side, voids were observed. At the anode side, a pileup of Pb was observed, indicating that Pb is the dominant diffusing species. The mean time to failure (MTTF) measured for the eutectic SnPb solder joint is far below the 10 000 h required by the packaging industry.

Eutectic SnPb lines in V grooves for electromigration study were conducted. Two Cu wires at both ends of the V groove served as electrodes.[56,57] A V-shaped solder line approximately 200 $\mu$m long, 100 $\mu$m wide, and around 67 $\mu$m deep is shown in Fig. 27(a). The lines were stressed at current density of $5\times10^4$A/cm$^2$ at room temperature as well as at 150 °C. Figures 27(b) and 27(c) illustrate scanning electronic microscope images of hump and void growth at room temperature after being stressed for 192 and 288 h, respectively. Both the accumulation at the anode side and the depletion at the cathode side grew bigger over time. Besides these morphological changes, compositional changes in the line were investigated.

For compositional analysis, a series of EDX spots along the solder line was performed on the surface as well as on the polished surfaces, which were about 14 and 24 $\mu$m below the original surface, and the results are plotted in Fig. 28(a). The amount of Sn at the anode side is consistently higher than that at the cathode side. The increase of Sn towards the cathode has occurred not only on the top surface but also on the polished surfaces, at a slower rate with increasing depth into the line, as shown in Fig. 28(a). In Fig. 28(b), the Sn change in concentration versus depth, in the vertical direction, near the anode side is shown.

The compositional profiles of Sn show that the electromigration of Sn atoms is against the concentration gradient of Sn (uphill diffusion). However, the concentration gradient exerts no driving force on the diffusion of Sn since there is no chemical potential gradient. We note that this is different from the effect of backstress in short strips of Al induced by electromigration.[64,65] Backstress produces a concentration gradient of vacancies along the strip, in turn, a atom flux opposing electromigration. It is also different from the classic Soret effect of thermomigration in solid solutions.[55] Here, the compositional change in the longitudinal direction is due to electromigration, but in the vertical direction it might include other forces due to the stress gradient or temperature gradient. However, if it is assumed that the surface of the sample serves as the source of vacancies

for Sn diffusion, it naturally leads to a redistribution of Sn in the vertical direction.

The finding that Sn and Pb are, respectively, the dominant diffusing species in electromigration at room temperature and at 150 °C,[56,73–75] is in agreement with a study of tracer diffusion in eutectic SnPb solder. The study showed that below 100 °C, Sn diffuses faster than Pb, but above 100 °C, Pb is the faster diffuser.[76] This behavior of crossover will impose a serious limitation on accelerated tests of electromigration in solder joints. Accelerated tests which are carried out at temperatures above 100 °C may not predict failure at temperatures below 100 °C. However, if the actual operating temperature of solder joints is close to 100 °C, there is no room for accelerated tests. No doubt, this is a challenging issue.

Another very unique and important electromigration behavior in solder joints is the polarity effect on IMC growth at the cathode and anode. Electromigration drives atoms from the cathode to the anode. Therefore, it tends to dissolve or retard the growth IMC at the cathode but build ups or enhances the growth IMC at the anode.[77,78] Figures 29(a) and 29(b) show SEM images of IMC $Cu_6Sn_5$ and $Cu_3Sn$ growth at the anode side in a eutectic SnAgCu V-groove sample with Cu electrodes. The sample was tested with current density of $3.2\times10^4$ A/cm$^2$ at 180 °C for 10 and 87 h, respectively. Figures 29(c) and 29(d) show corresponding images at the cathode side. The IMC at the anode is much thicker than that at the cathode. In Fig. 29(d), voids can be seen between the solder and the IMC.

When a thin film UBM is used at the cathode, dissolution of the thin film UBM into the solder and being driven toward the anode due to electromigration are other reliability issues. Since noble and near-noble metals are known to diffuse interstitially in solder alloys, the effect of electromigration of these metals in a solder alloy is extremely fast.[79–81]

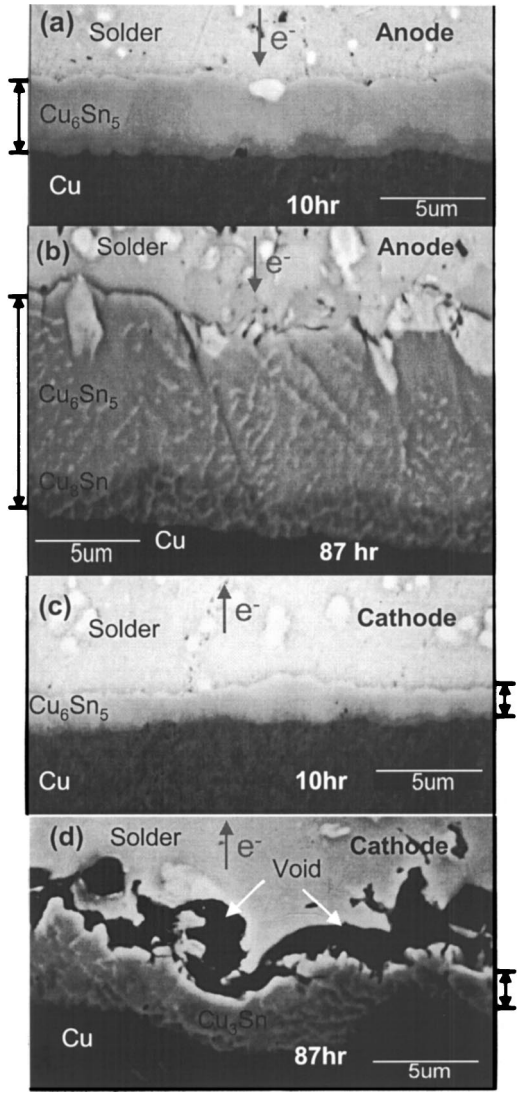


FIG. 29. SEM images of IMC $Cu_6Sn_5$ and $Cu_3Sn$ growth at the anode and cathode in a eutectic SnAgCu V-groove sample with Cu electrodes; the sample was tested with current density of $3.2\times10^4$ A/cm$^2$ at 180 °C. (a) anode side after 10 h, (b) anode side after 87 h, (c) cathode side after 10 h, and (d) cathode side after 87 h (after Ref. 78).

### E. High temperature Pb-free solders

In Fig. 1(b), we showed a two-level packaging structure using a high–low combination of solder joints of 95Pb5Sn and eutectic SnPb. At present, there are Pb-free solders which can replace eutectic SnPb, but there is none to replace high Pb. We listed 80Au20Sn with a eutectic point of 280 °C, yet this eutectic alloy is known to have poor reflow properties because it does not react readily with Cu or Ni. The Sn in the alloy tends to stay with Au because it is a eutectic consisting of two Au–Sn compounds. In order to react with Cu or Ni, the Sn atoms must dissociate themselves from the Au atoms, so that the driving force is reduced. On the other hand, a eutectic alloy having pure Sn as a eutectic component is much more reactive, but it will have a melting point less than that of pure Sn. Among the eutectic alloys of Sn and noble metals, we know very little about the binary systems of Sn–Rh, Sn–Ir, and Sn–Os. Their binary phase diagrams are unavailable.

## VII. SUMMARY

The study of solder reaction was a low cost research project. The solder flux serves as a poor-man's vacuum ambient. One can start a solder project with a hot plate, a polishing wheel, and an optical microscope.[82] In this review we discussed the metallurgical reliability issues or microstructure changes of flip chip solder joints when they are subjected to chemical, mechanical, electrical, and thermal forces. Due to the trend towards miniaturization, these issues will become more serious. In advanced Cu/low $k$ (dielectric constant) interconnects, we must not allow molten solder to wet Cu lines. The weak mechanical properties of low $k$ materials may be incompatible with the large thermal strain in solder bumps as mentioned. *In situ* study of the solder wetting reaction is of interest, e.g., using synchrotron radiation. Numerical simulation of reliability behavior of solder joints under multiple driving forces will be of great value to industry. For applications in mainframe computers, aerospace and military equipment, and high temperature devices, the elec-

tronic industry cannot give up the reliability of Pb-containing solders because of environmental concerns, So Pb-free research should still be active for a while.

## ACKNOWLEDGMENTS

The authors would like to thank W. J. Choi [University of California, Los Angeles (UCLA)] and Zhang Fan [Institute of Materials Research and Engineering] for assistance and for preparing the figures. One author (K.N.T.) would like to acknowledge support by NSF Contract No. DMR-9987484 and SRC Contract No. NJ-774 and to thank his students, post doctoral students, and visitors for their valuable contributions to the study of Pb-free solder metallurgy (H. K. Kim, Y. Wang, Ann Liu, Jessica Almaraz, Fiona Ku, P. G. Kim, Chih Chen, D. W. Zheng, C. Y. Liu, W. J. Choi, H. Gan, G. Z. Pan, J. W. Jang, E. C. C. Yeh, and K. Zeng).

[1] *International Technology Roadmap for Semiconductors* (Semiconductor Industry Association, San Jose, CA, 2001); see http://public.itrs.net/.
[2] K. Puttlitz and P. A. Totta, *Area Array Interconnection Handbook* (Kluwer Academic, Boston, MA, 2001).
[3] K. N. Tu and K. Zeng, Mater. Sci. Eng., R. **34**, 1 (2001).
[4] J. Cannis, Adv. Packaging **8**, 33 (2001).
[5] See lead-free.org/legislation and www.nemi.org/PbFreepublic.
[6] J. F. Ziegler and G. R. Srinivasan, IBM J. Res. Dev. **40**, 1 (1996).
[7] H. K. Kim, H. K. Liou, and K. N. Tu, J. Mater. Res. **10**, 497 (1995).
[8] K. Zeng and K. N. Tu, Mater. Sci. Eng., R. **38**, 55 (2002).
[9] C. M. Miller, I. E. Anderson, and J. F. Smith, J. Electron. Mater. **23**, 595 (1994).
[10] D. R. Frear, JOM **48**, 49 (1996).
[11] K. W. Moon, W. J. Boettinger, U. R. Kattner, F. S. Biancaniello, and C. A. Handwerker, J. Electron. Mater. **29**, 1122 (2000).
[12] M. E. Loomas and M. E. Fine, Metall. Mater. Trans. A **31A**, 1155 (2000).
[13] W. Peng, M.Sc. thesis, Helsinki University of Technology, Helsinki, Finland, 2001.
[14] H. K. Kim, H. K. Liou, and K. N. Tu, Appl. Phys. Lett. **66**, 2337 (1995).
[15] H. K. Kim and K. N. Tu, Phys. Rev. B **53**, 16027 (1996).
[16] P. G. Kim, J. W. Jang, T. Y. Lee, and K. N. Tu, J. Appl. Phys. **86**, 6746 (1999).
[17] A. A. Liu, H. K. Kim, K. N. Tu, and P. A. Totta, J. Appl. Phys. **80**, 2774 (1996).
[18] H. K. Kim, K. N. Tu, and P. A. Totta, Appl. Phys. Lett. **68**, 2204 (1996).
[19] B. S. Berry and I. Ames, IBM J. Res. Dev. **13**, 286 (1965).
[20] C. Y. Liu, K. N. Tu, T. T. Sheng, C. H. Tung, D. R. Frear, and P. Elenius, J. Appl. Phys. **87**, 750 (2000).
[21] M. Li, F. Zhang, W. T. Chen, K. Zeng, K. N. Tu, H. Balkan, and P. Elenius, J. Mater. Res. **17**, 1612 (2002).
[22] R. A. Gagliano and M. E. Fine, JOM **6**, 33 (2001).
[23] P. Oberndorff, Ph.D. thesis, Technical University of Eindhoven, Eindhoven, The Netherlands, 2001, Chap. 7.
[24] K. N. Tu, T. Y. Lee, J. W. Jang, L. Li, D. R. Frear, K. Zeng, and J. K. Kivilahti, J. Appl. Phys. **89**, 4843 (2000).
[25] T. Y. Lee, W. J. Choi, K. N. Tu, J. W. Jang, S. M. Kuo, J. K. Lin, D. R. Frear, K. Zeng, and J. K. Kivilahti, J. Mater. Res. **17**, 291 (2002).
[26] C. H. Ma and R. A. Swalin, Acta Metall. **8**, 342 (1960).
[27] H. K. Kim and K. N. Tu, Appl. Phys. Lett. **67**, 2002 (1995).
[28] I. M. Lifshiz and V. V. Slezov, J. Phys. Chem. Solids **19**, 35 (1961).
[29] C. Wagner, Z. Elektrochem. **65**, 581 (1961).
[30] V. V. Slezov, *Theory of Diffusion Decomposition of Solid Solutions* (Harwood Academic, 1995), pp. 99–112.
[31] A. M. Gusak and K. N. Tu, Phys. Rev. B **66**, 115403 (2002).
[32] K. N. Tu, F. Ku, and T. Y. Lee, J. Electron. Mater. **30**, 1129 (2001).
[33] J. H. Lee, J. H. Park, Y. H. Lee, Y. S. Kim, and D. H. Shin, J. Mater. Res. **16**, 1227 (2001).
[34] F. H. Howie and E. D. Hondros, J. Mater. Sci. **17**, 1434 (1982).
[35] D. W. G. White, Metall. Trans. **2**, 3067 (1971).
[36] T. Young, Philos. Trans. R. Soc. London **95**, 65 (1805).
[37] P. G. de Gennes, Rev. Mod. Phys. **57**, 827 (1985).
[38] Y. Wang, H. K. Kim, H. K. Liou, and K. N. Tu, Scr. Metall. Mater. **32**, 2087 (1995).
[39] P. G. Kim and K. N. Tu, Mater. Chem. Phys. **53**, 165 (1998).
[40] B. G. Bader, Weld. J. (Miami) **48**, 551 (1969).
[41] C. Y. Liu and K. N. Tu, Phys. Rev. E **58**, 6308 (1998).
[42] E. W. Washburn, Phys. Rev. **17**, 273 (1921).
[43] J. A. Mann, Jr., L. Romero, R. R. Rye, and F. G. Yost, Phys. Rev. E **52**, 3967 (1995).
[44] R. R. Rye, F. G. Yost, and J. A. Mann, Jr., Langmuir **12**, 4625 (1996).
[45] W. B. Harding and H. B. Pressly, American Electroplating Society, 50th Annual Proceedings, 1963, p. 60.
[46] W. A. Mulholland and D. L. Willyard, Weld. Res. (Miami) **54**, 466s (1974).
[47] H. P. Kehrer and E. W. Wenzel, Metall. **30**, 1047 (1979).
[48] C. Herring and J. K. Galt, Phys. Rev. **85**, 1060 (1952).
[49] F. R. N. Nabarro and P. J. Jackson, in *Growth and Perfection of Crystals*, edited by R. H. Doremus, B. W. Roberts, and D. Turnbull (Wiley, New York, 1958), p. 12.
[50] W. C. Ellis, D. F. Gibbons, and R. C. Treuting, in Ref. 49, p. 102.
[51] K. N. Tu, Phys. Rev. B **49**, 2030 (1994).
[52] G. T. T. Sheng, C. F. Hu, W. J. Choi, K. N. Tu, Y. Y. Bong, and L. Nguyen, J. Appl. Phys. **92**, 64 (2002).
[53] W. J. Choi, T. Y. Lee, K. N. Tu, N. Tamura, R. S. Celestre, A. A. MacDowell, Y. Y. Bong, L. Nguyen, and G. T. T. Sheng, 52nd ECTC Proceedings, San Jose, CA, 2002, p. 628.
[54] Y. Kariya, C. Gagg, and W. J. Plumbridge, Solder Surf. Mount Tech. **13**, 39 (2001).
[55] Q. T. Huynh, C. Y. Liu, C. Chen, and K. N. Tu, J. Appl. Phys. **89**, 4332 (2000).
[56] G. Xu, M.Sc. thesis, University of California, Los Angeles, 2001.
[57] P. G. Shewman, *Diffusion in Solids*, 2nd ed. (The Minerals, Metals, and Materials Society, Warrendale, PA, 1989), Chap. 7.
[58] J. W. Jang, C. Y. Liu, P. G. Kim, K. N. Tu, A. K. Mal, and D. R. Frear, J. Mater. Res. **15**, 1679 (2000).
[59] Y. Guo, W. T. Chen, and C. K. Lim, Proceedings of the ASME Conference on Electronic Packaging, San Jose, CA, 1992, p. 199.
[60] Y. Guo, C. K. Lim, W. T. Chen, and C. G. Woychik, IBM J. Res. Dev. **37**, 17 (1993).
[61] B. Han and Y. Guo, J. Electron. Packag. **117**, 185 (1995).
[62] H. B. Huntington and A. R. Grone, J. Phys. Chem. Solids **20**, 76 (1961).
[63] F. M. d'Heurle and R. Rosenberg, *Physics of Thin Films* (Academic, New York, 1973), Vol. 7, p. 257.
[64] I. A. Blech, J. Appl. Phys. **47**, 1203 (1976).
[65] I. A. Blech and C. Herring, Appl. Phys. Lett. **29**, 131 (1976).
[66] F. M. d'Heurle and P. S. Ho, in *Thin Films: Interdiffusion and Reactions*, edited by J. M. Poate, K. N. Tu, and J. W. Mayer (Wiley–Interscience, New York, 1978), p. 243.
[67] P. S. Ho and T. Kwok, Rep. Prog. Phys. **52**, 301 (1989).
[68] K. N. Tu, Phys. Rev. B **45**, 1409 (1992).
[69] J. R. Lloyd and J. J. Clement, Thin Solid Films **262**, 135 (1995).
[70] C. K. Ho and J. M. E. Harper, Mater. Chem. Phys. **52**, 5 (1998).
[71] P. C. Wang, G. S. Cargill III, I. C. Noyan, and C. K. Hu, Appl. Phys. Lett. **72**, 1296 (1998).
[72] E. C. C. Yeh, W. J. Choi, and K. N. Tu, Appl. Phys. Lett. **80**, 580 (2002).
[73] S. Brandenburg and S. Yeh, Proceedings of the Surface Mount International Conference and Exposition, San Jose, CA, p. 337.
[74] T. Y. Lee, K. N. Tu, and D. R. Frear, J. Appl. Phys. **90**, 4502 (2001).
[75] C. Y. Liu, C. Chen, C. N. Liao, and K. N. Tu, Appl. Phys. Lett. **75**, 58 (1999).
[76] D. Gupta, K. Vieregge, and W. Gust, Acta Mater. Met. **47**, 5 (1999).
[77] S. W. Chen, C. M. Chen, and W. C. Liu, J. Electron. Mater. **27**, 1193 (1998).
[78] H. Gan, W. J. Choi, G. Xu, and K. N. Tu, JOM **6**, 34 (2002).
[79] C. K. Hu and H. Hungtington, Phys. Rev. B **26**, 2782 (1982).
[80] C. K. Hu and H. Hungtington, Phys. Rev. B **28**, 579 (1983).
[81] C. K. Hu and H. Hungtington, J. Appl. Phys. **58**, 2564 (1985).
[82] Y. Wang and K. N. Tu, Appl. Phys. Lett. **67**, 1069 (1995).